Chem Soc Rev

REVIEW ARTICLE

View Article Online
View Journal | View Issue

Cite this: *Chem. Soc. Rev.*, 2015, **44**, 8576

In vivo delivery, pharmacokinetics, biodistribution and toxicity of iron oxide nanoparticles

Hamed Arami,[a] Amit Khandhar,[c] Denny Liggitt*[b] and Kannan M. Krishnan*[a]

Received 9th July 2015

DOI: 10.1039/c5cs00541h

www.rsc.org/chemsocrev

Iron oxide nanoparticles (IONPs) have been extensively used during the last two decades, either as effective bio-imaging contrast agents or as carriers of biomolecules such as drugs, nucleic acids and peptides for controlled delivery to specific organs and tissues. Most of these novel applications require elaborate tuning of the physiochemical and surface properties of the IONPs. As new IONPs designs are envisioned, synergistic consideration of the body's innate biological barriers against the administered nanoparticles and the short and long-term side effects of the IONPs become even more essential. There are several important criteria (*e.g.* size and size-distribution, charge, coating molecules, and plasma protein adsorption) that can be effectively tuned to control the *in vivo* pharmacokinetics and biodistribution of the IONPs. This paper reviews these crucial parameters, in light of biological barriers in the body, and the latest IONPs design strategies used to overcome them. A careful review of the long-term biodistribution and side effects of the IONPs in relation to nanoparticle design is also given. While the discussions presented in this review are specific to IONPs, some of the information can be readily applied to other nanoparticle systems, such as gold, silver, silica, calcium phosphates and various polymers.

1. Introduction

Superparamagnetic iron oxide (γ-Fe_2O_3 and Fe_3O_4) nanoparticles (IONPs) are biocompatible, biodegradable and non-toxic and have been used for a wide range of biomedical applications such as tumors or vascular imaging,[1–3] drug delivery,[4] gene therapy,[5]

[a] *Department of Materials Science and Engineering, University of Washington, Seattle, Washington, 98195, USA. E-mail: kannanmk@uw.edu*
[b] *Department of Comparative Medicine, University of Washington School of Medicine, Seattle, Washington, 98195, USA. E-mail: dliggitt@uw.edu*
[c] *Lodespin Labs, PO Box 95632, Seattle, WA, 98145, USA*

Hamed Arami

Hamed Arami is the recipient of Stanford Cancer Imaging Training (SCIT) post-doctoral fellowship award. He obtained his dual PhD from Departments of Materials Science and Engineering (MSE) and Nanotechnology and Molecular Engineering (NTME) at University of Washington in 2015. His research is focused on various aspects of biomaterials design and their in vitro and in vivo applications. He is currently exploring potential strategies to expedite translation of iron oxide nanoparticles to clinics for different diagnostic and therapeutic purposes. His main research interests are development of advanced biomaterials (nanoparticles, hydrogels and scaffolds) for biomedical imaging, targeted therapy, tissue engineering and regenerative medicine.

Amit Khandhar

Dr Khandhar earned his PhD from the University of Washington in 2013. His research in the design and synthesis of superparamagnetic iron oxide nanoparticles for Magnetic Fluid Hyperthermia (MFH) and Magnetic Particle Imaging (MPI) was critical in the founding of Lodespin Labs – a life sciences venture committed to translational applications of iron oxide nanoparticles. Currently, as a co-founder of Lodespin Labs, Dr Khandhar leads pharmacologic evaluation of magnetic nanoparticle tracers for enabling clinical applications in the emerging MPI imaging modality.

in vivo tracking of labeled cells,[6] magnetic separation of cells or molecules,[7] or as an iron supplement for patients with anemia.[8] Immediately after their administration *in vivo*, a host of innate immunological mechanisms start to recognize and collect these foreign particles and direct them to the major elimination pathways of the body.[9] Therefore, there is always a competition between the desired distributions of the IONPs in specific organs and their highly active clearance mechanisms.[10] The amount and distribution pattern of the IONPs in different organs and tissues, during or after any clinical diagnostic or therapeutic application, is generally considered as biodistribution and the rate of their recognition and removal by the immune system, metabolism and excretion from the body is usually referred to as pharmacokinetics. Knowing these two parameters is crucial to enhance the expected functionality of the IONPs in any selected region or organ of the body and to minimize their toxicological side effects due to any undesirable biodistribution or pharmacokinetic behavior.[11]

Recent progress in synthesis, characterization and most importantly, surface functionality of the IONPs have enabled researchers to improve these two important parameters and answer some important questions related to their clinical applications.[12] It is well known that whilst the size of the iron oxide crystals determines the magnetic properties of IONPs, the additional molecules on their surface act as the main interface between the IONPs and the body's immune system.[1] Therefore, depending on how the IONPs were synthesized, their surface chemistry, the desired application and administration methods, the expected pharmacokinetic and biodistribution behavior of the IONPs may be different.[13]

Iron oxide nanoparticles are prepared by two major chemical methods. Co-precipitation of Fe^{2+} (ferrous) and Fe^{3+} (ferric) ions in an alkaline solution is a well-established conventional IONPs synthesis method.[14] Further, these IONPs can be coated *in situ* with different types of polymers (*e.g.* dextran,[15] chitosan[4] and starch[16]) by the synthesis of the IONPs in the presence of these molecules in solution. These types of IONPs have been extensively investigated during the last two decades and have been successfully translated to the clinic.[17] While the method can be easily scaled up for mass production of the IONPs, it is difficult to obtain uniform iron oxide core sizes with narrow size distributions and controlled magnetic properties using such aqueous co-precipitation methods.[4] Alternatively, thermal decomposition of organic complexes of iron (*e.g.* iron pentacarbonyl, iron oleate or FeOOH) in the presence of capping agents (*e.g.* oleic acid and oleyl amine), results in excellent control of size, shape and monodispersity of the IONPs, and the desired magnetic properties.[18–21] The main drawback of this approach is the hydrophobicity of the synthesized IONPs, which requires elaborate, multi-step surface modifications to transfer them to aqueous media and improve their bio-functionality.[4,12]

This paper provides a comprehensive review of the *in vivo* biological barriers encountered by IONPs. Furthermore, parameters that play key roles in the clearance pathways, body distribution and ultimate fate of IONPs are discussed. We will show that synergistic consideration of all these parameters is

Denny Liggitt

Denny Liggitt, DVM, PhD is a Professor and Chairman of the Department of Comparative Medicine, School of Medicine, University of Washington (UW), Seattle. He is a board-certified comparative pathologist who also serves as an advisor to the UW Institute of Translational Health Sciences as well as several other entities. Professor Liggitt is an authority in the development and evaluation of animal models of human diseases and has published more than 180 scientific papers in this and related areas. Research interests are principally directed toward projects involving, in a broad sense, in vivo interactions of the host with its defense and steady-state mechanisms and the role that selected cytokines and growth factors play in this interaction. He has particular expertise in the pre-clinical development, evaluation, and approval of biologic-based drugs. He has been involved in fostering several biotech companies and translating several discoveries through pre-clinical development.

Kannan M. Krishnan

Kannan M. Krishnan obtained his PhD (1984) from UC, Berkeley and is presently Professor of Materials Science at the University of Washington, Seattle. His research is broadly in Bioengineering at the intersection of Magnetism, Materials and Medicine focusing on diagnostics, imaging and therapy, with appropriate translational research and commercialization activities. His many recognitions include the IEEE Fink Prize (2012) and Distinguished Lecturer Award (2009), Guggenheim (2004) and Rockefeller (2008) Fellowships, the Burton Medal (MSA, 1992), and the College of Engineering Outstanding Educator Award (UW, 2004). He is an elected Member of the Washington State Academy of Science, and Fellow of the American Association for the Advancement of Science, the American Physical Society, the Institute of Physics (London), and the Institute of Electrical and Electronics Engineers (IEEE). In 2010, he founded a start-up company, LodeSpin Labs, involved in the development of tailored magnetic carriers for a range of biomedical applications.

required in order to develop standard criteria for tuning the pharmacokinetics and biodistribution of the IONPs for a specific clinical application. The interpolation of this carefully classified information to future studies will help decrease costs associated with clinical trials and potentially reduce the number of animal studies by avoiding unnecessary experiments. Also, it can expedite the clinical translation of the IONPs to various imaging or therapeutic applications (*e.g.* early diagnosis and treatment of cancers, heart and brain plaques and lesions and efficient regenerative tissue engineering). Additionally, pharmacokinetics, biodistribution and clearance pathway of the IONPs administrated through various *in vivo* routes such as intravenous and retro-orbital injection, intrapulmonary or oral delivery, will be discussed along with their physiological limitations and the IONPs properties required for each one of them. Recent progress in successful clinical applications of IONPs and any reported side-effects on humans will be also discussed in detail.

2. IONPs pharmacokinetics

Depending on the desired biomedical applications, iron oxide nanoparticles have been mostly administrated through intravenous injection (IV), oral delivery or intranasal (inhalation) pathway (also see Section 2.2). Regardless of the biological barriers (*e.g.* acidic gastric pH and the general stability of the IONPs) specific to each administration method, the body's immune system responds quickly to the presence of IONPs, trying to eliminate them through phagocytic, metabolic and degradative processes in immune cells (*i.e.* circulating white blood cells such as monocytes and residential tissue macrophages). Based on previous reports, summarized in this review, tissue (*e.g.* liver and spleen) macrophages are the most critical cells in the elimination of IONPs from the blood circulation. In this section, we describe the pharmacokinetic performance and the desired characteristics of the IONPs for each administration method.

2.1 Intravenously injected IONPs

Intravenous injection is the most commonly used approach for administration of IONPs, specially for their use as MRI contrast agents. Basic characteristics of some of the IONPs that are approved for clinical use as intravenously injected contrast agents for MRI are shown in Table 1. In the 1990's, ultrasmall superparamagnetic iron oxide (USPIO) nanoparticles were developed for diagnostic and therapeutic clinical applications by Weissleder *et al.*[22] and other research groups,[23] with the most commonly used ones being AMI-227 (Sinerem® by Guerbet and Combidex® by Advanced Magnetics, also called as monocrystalline iron oxide nanoparticle or MION[23,24]), SHU55C (Schering AG) and NC100150 (Clariscan, Nycomed). Compared to the first generation of IONPs with hydrodynamic size, $d_H \sim$ 150 nm, USPIOs were smaller ($d_H \sim$ 20–30 nm) and showed a longer blood circulation time (*e.g.* 4 h 30 min in rats).[25,26] This enabled the use of USPIOs extensively as blood pool MRI contrast agents. Later, cross-linked iron oxide (CLIO) nanoparticles were prepared to prevent the detachment of the dextran coating because of its weak bonding with hydroxyl groups on the surface of the IONPs.[27] In contrast to USPIOs, CLIO series of IONPs had several iron oxide crystallites as their core.[27] This group of IONPs has also been widely investigated for different types of biomedical imaging applications. Further, for each application, it is important to know the blood circulation time of the injected IONPs (*i.e.*, the time between injection and elimination from the blood) and utilize this data to tune the IONPs characteristics based on the desired circulation time for that specific application.

2.1.1 Blood half-life. Blood or plasma half-life ($t_{1/2}$) of the NPs is the time it takes for the concentration of the injected NPs in the blood to decrease to half its initial value and is a helpful measure to monitor the pharmacokinetics of the NPs. This decrease in concentration is due to the elimination of the NPs through various organs (details to be discussed in the next sections of this review). For magnetic nanoparticles (*i.e.* IONPs) the half-life can also be defined as the time in which the MRI T_2 or T_1 relaxation rates of the blood reduces to half its initial value immediately after the injection of the NPs.[28,29] Assuming a one-compartment pharmacokinetic model for IONPs, *i.e.* they do not disintegrate after injection and their distribution in blood after injection remains uniform, the decrease in concentration often follows a mono-exponential decay function (eqn (1)). A simple fitting of the data (*e.g.* IONPs concentrations or changes in MRI contrast or fluorescent signal intensity of the blood samples) to this equation is used to calculate half-life ($t_{1/2}$) accurately (eqn (2)).[16,22] The general form of the expression is as follows:

$$\mathrm{ED} = \mathrm{ID}\exp(-t \times R) \quad (1)$$

where, R is the elimination rate constant, ED is the effective dose (the dose remaining in the blood plasma at the desired therapeutic time point, t) and ID is the injected dose. From eqn (1), we get the following expression for the blood half-life ($t_{1/2}$):[23]

$$t_{1/2} = \frac{\ln(2)}{R} \quad (2)$$

The blood half-life of different types of IONPs, shown in Table 1, ranges from several minutes[22] to several days[30] in rodents and from 1 hour (VSOP-C184)[31] to 24 hours (AMI-227)[32] in humans. Further, blood half-life values are highly dependent on dose levels of the injected IONPs (this parameter is discussed later in Section 2.1.4).

2.1.2 Mononuclear phagocytic system (MPS): the major clearance route. Intravenously injected IONPs, are selectively taken up by the liver and spleen, with few reports also showing the presence of a smaller fraction of the injected IONPs in the lung.[69,70] Liver and spleen are, in fact, the major clearance pathways for the IONPs in the blood and these organs form part of the important immune system known as mononuclear phagocytic system (MPS) or monocyte–macrophage system also known classically as reticuloendothelial system (RES).[71,72] In this section, details about the various physiological components of the MPS and their role in the clearance pathways are provided.

Table 1 Blood half-lives ($t_{1/2}$) of the different types of iron oxide nanoparticles (IONPs) after their injection into animal models or human. The iron dosages are reported here based on mg Fe kg^{-1} body weight unit for easier comparison

CS/HS	Coating molecule	Name	Charge (mV)	Model	Dose (mg Fe kg^{-1})	$t_{1/2}$	Applications/notes	Ref.
4–7/72	Dextran	SPIO (AMI25)	NA	Rats	0.224	6 min	General MRI	22
4–6/150					1.12	16 min	applications	23
4–6/20		USPIO (AMI 227)	NA		1.12	2 h		23
4–7/17		MION-46	NA		0.224	81 min	MRI/made by size fractionation of AMI-25	22 and 33
4–6/NA		USPIO	NA		15	2 h	MRI of spinal cord	34
NA/35		Ferumoxtran-10 (Sinerem)	NA	Rabbits	56	Several days	MRI of atherosclerotic plaque	35 and 36
5/30			NA	Human	2.6	21–30 h	MRI of lymph nodes	37
5/30		BMS 180549/	NA	Rats	0.14–1.68	3.7 h	General MRI evaluation	38
		USPIO	NA	Human	1.7	>24 h	General MRI evaluation	32
5/30		USPIO sinerem	NA	Rats	11.2	4 h 30 min	Tumor MRI	26
4–6/227		Ferumoxides (Feridex) or endorem	NA	Human	0.56–0.84	2 h	Liver MRI	39
NA/121		Feridex	NA	Rabbits	4.8	0.46 h	MR imaging of	40
NA/15		Fractionated Feridex				15.9 h	atherosclerosis	
NA/50–80	Dextran (20 kDa)	Amino-dextran SPIO-micromod	−4.95 to −0.77	Mice	4	5–60 min	Protein adsorption analysis	41
12/50	Dextran (40 kDa)	NA	0	Rats	5	50 min	MRI of myocardial infarction and brain tumor	42 and 43
3–5/60–80	Carboxy dextran	SHU 555 C (Resovist)	Anionic	Rats	5.6	56 ± 17 min	Imaging of inflammatory bowel disease	44
				Rats	2.8	35 min	General MRI	45
				Human	NR	6 h	applications	
NA/25		SPIO	−20	Rats	11.2	90 min	MR lymphography	46
		USPIO	NA	Rabbits		6 h	MRI of atherosclerotic plaques	47
7/30		Ferumoxytol (AMI7228)	Anionic	Human	<4	10–14 h	MR angiography	45 and 48
				Rats	2.24	67 min		45
20/42	Dextran + antibody	Ocean nanotech	NA	Mice	NR	7.5 h	Brain tumor targeting and MRI (0.2 mL, concentration NR)	49
30/30 × 70	Dextran-PEG	Nanoworms	NA	Mice	3	16–19 h	Tumor targeting	50
NA/30	Dextran-PEG +	NA	NA			17.9–19.6 h		
NA	targeting molecule	Nanoworms	NA	Mice	3.3[a]	12 h[b]	Atherosclerotic plaques/one dimensional clusters with 80–110 nm length and 30 nm width	51
NA/250	Cross-linked dextran (20 kDa)	Nanoworms	NA	Mice	~5[a]	10 h	MRI, protein adsorption and blood half-life analysis	52
5–7/20	Starch	FeO–BPA	NA	Pigs	4	150 min	Abdominal MR	53
				Rodents	1–3	45–100 min	angiography	
NA/60–90		NA	−12.3 to 3.9	Rats	11.2	13 min	MR lymphography	46
5–7/20	PEG + starch	NC100150	Anionic	Rabbits	0.25–1	45–120 min	MRI of renal perfusion	54
5–7/25		(Clariscan)		Human	3–4	3–4 h	MR angiography	55
<10/142	PEG (5 kDa)–starch[c]	NA	+24.4	Rats	12	7.29 h	Tumor targeting-by increasing the PEG MW to 20 kDa, HS and half-life increased to 168 nm 11.75 h	16
7/30	Chitosan-PEG–chlorotoxin-cy5.5	NA	0	Mice	6.7[a]	7–8 h	Cancer targeting and imaging/NIR fluorescence scanner for half blood life	56
5/10	PEG + lipid	NA	NA	Rats	6	45 min	Kidney targeting/imaging (γ-Fe_2O_3 core crystals)	57
10–15/35		LSPIO	NA	Mice	3.9	1.02 h[b]	MRI detection of atherosclerotic lesions/the	58
NA/10		LUSPIO	NA			1.52 h[b]		
10–15/36	PEG + lipid +	LSPIO	NA			7.28–7.42 h[b]	Half-lives in wild type	
NA/12–16	antibody	LUSPIO	NA			9–9.3 h[b]	mice reduced to 1.01	

Table 1 (*continued*)

CS/HS	Coating molecule	Name	Charge (mV)	Model	Dose (mg Fe kg^{-1})	$t_{1/2}$	Applications/notes	Ref.
							(no targeting) and 1.12 (with targeting) for LSPIO and reduced to 1.41 (no targeting) and 1.55 (with targeting) for LUSPIO	
4/8.6	Citrate coating	VSOP-C184	NA Pigs	Rats	2.52	21 ± 5 min 36 ± 4 min	MRI pre-clinical characterizations	59
4/7			NA	Human	0.84–4.2	0.5–1.5 h	General MRI applications	31
NA/12		VSOP-C43	NA	Rats	1.68	8.4 ± 0.9 min	Effect of age on half-life/half-life increased to 15.9 ± 2.4 in old rats	60
19.6/117.3	PEG + polyaniline + BCNU drug	NA	NA	Mice	15	62 h[d]	Brain tumor imaging and drug delivery	30
8/24	DMSA	NA	Anionic	Mice	22.4	Several hours	Tumor MRI and targeting (maghemite core crystals)	61
12/42	DMSA	NA	−35	Rats	5	10 min	General MRI application/highly monodisperse cores	62
12/49	DMSA–PEG (2 kDa)		−15			20 min		
17/86	PMAO–PEG (5 kDa)	NA	Neutral	Mice	7	4 min	Designed for magnetic particle imaging (MPI)/highly monodisperse cores	63 and 64
20/42						19 min		
27/78	PMAO–PEG (20 kDa)					160 min		
19.7/98	PEG	NA	−3 to −7	Mice	7	12–14 min		65
19.7/43						12–14 min		
10/63	Polyacrilamide + PEG (0, 0.6, 2, 10 kDa)	NA	NA	Rats	7	28, 25, 38 and 150 min	Brain tumor MRI/larger PEG MWs increase the half-life time	66
4–8/21	Phosphonate	P904	NA	Rabbits	56	3.5 h	MRI of atherosclerotic plaques	35 and 36
70/NA	Silica + PEG	NA	NA	Rats	5.7	2.5 h	General MRI	29
NA/1.6 min	P(S/V–COOH) polymer	MPIO-bangs	NA	Mice	0.0145	1 min	MRI of myocardial infarction	67 and 68

Abbreviations: [core size and hydrodynamic size (CS/HS)], [blood half-life ($t_{1/2}$)], [not available (NA)], [monocrystalline iron oxide nanoparticles (MION)], [lipid-coated ultra-small superparamagnetic iron particles (LUSPIOs)], [larger lipid-coated superparamagnetic iron oxide particles (LSPIOs)], [*meso*-2,3-dimercaptosuccinic acid (DMSA)], [1,3-bis(2-chloro-ethyl)-1-nitroso-urea (BCNU)], [poly(maleic anhydride-*alt*-1-octadecene) (PMAO)]. [a] Assuming that each mouse weighed 30 g. [b] IONPs injected through retro-orbital route. [c] cross-linked starch. [d] Half-life reported for the BCNU drug loaded to the IONPs.

Later (Section 2.1.4), we will consider the physicochemical properties of IONPs (*e.g.* size, surface charge, surface coating density) that affect their biodistribution and clearance by the MPS.[73]

The MPS system includes monocytes circulating in the blood and macrophages located in different organs, such as liver, spleen, lymph nodes, bone marrow, lung and brain.[74] Generally, macrophage precursor cells form from hematopoietic stem cells in bone marrow and then get released into circulation as monocytes. These circulating monocytes then extravasate through the endothelium and migrate to tissues followed by differentiation into various larger size macrophage subsets, depending on their anatomical location and functional phenotype.[75] The major specialized tissue-resident macrophages are Kupffer cells in liver, alveolar macrophages in lungs, osteoclasts in bones and histiocytes in interstitial connective tissues. Distinct macrophage populations also exist in secondary lymphoid organs, including the macrophages residing in spleen marginal zones and sub-capsular sinus macrophages in lymph nodes. Tissue-specific macrophages also patrol highly immune-privileged organs such as brain (microglia), eyes and testes.[76] All these tissue-distributed macrophages clear the body of the presence of pathogens or foreign bodies such as bacteria, viruses, abnormal and old cells and IONPs, by phagocytosis (*i.e.* engulfing them followed by their degradation and metabolism, as discussed in Section 3), or by recruiting additional macrophages from circulation (during infections or injuries).[77]

In general, liver and spleen are usually the dominant organs for clearance of the nanoparticles from the bloodstream.[56] However, when injected in high dosages, the liver and spleen macrophages can only eliminate a fraction of the IONPs from the bloodstream and the excess IONPs get accumulated in other macrophage-rich tissues such as lung and adipose tissue.[78] Uptake of the IONPs by the macrophages of liver and spleen is usually preceded by (a) opsonization, (b) recognition by the macrophages and (c) phagocytosis (Fig. 1). Briefly, during the opsonization process, plasma proteins deposit on the surface of the injected IONPs, a process similar to other immunogenic species (*e.g.* viruses and bacteria) and one that

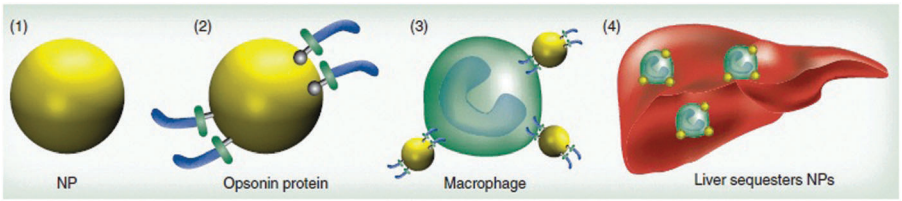

Fig. 1 Adsorption of the plasma proteins on the IONPs followed by their uptake by Kupffer cells and their accumulation in liver; presence of PEG prevents the opsonization and decreases the uptake of the IONPs by macrophages. Re-printed with permission from ref. 99. Copyright 2011, Future Medicine.

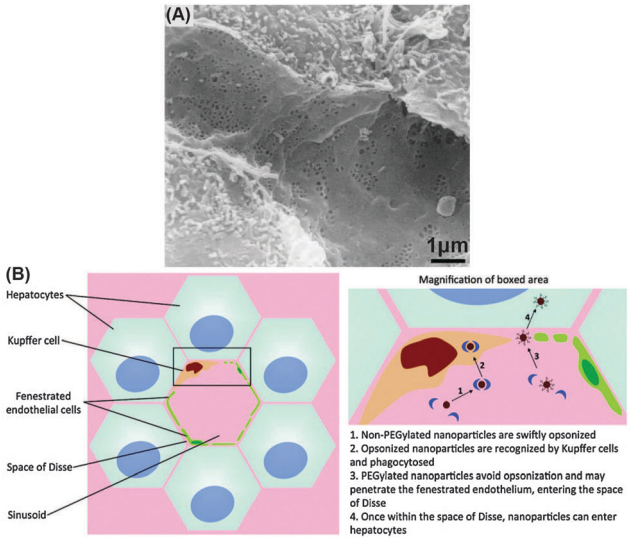

Fig. 2 (A) Scanning electron microscopy (SEM) image of the liver sinusoids. (B) Kupffer cells located in liver sinusoids phagocytize the IONPs from the bloodstream. Adapted with permission from ref. 100 and 106. Copyrights 2002, Elsevier B. V. and 2011, American Chemical Society.

specifically signals the Kupffer or reticular macrophages to recognize and eliminate them from the circulation.[27,28]

Kupffer cells are located inside the sinusoidal blood vessels of the liver (Fig. 2) and are the most active phagocytes in uptaking the IONPs. Kupffer cells first attach themselves to the approaching IONPs. Then they form foot-like extrusions around the IONPs, called pseudopodia, and encapsulate them in phagocytic vesicles or phagosomes. The wall of the phagosomes comes in contact with lysosomes, which are intracellular organelles containing an acidic environment responsible for degradation and metabolism of internalized species, and their membranes fuse with each other. Then, digestive enzymes are released from the lysosomes, which degrade the IONPs. The exact intracellular degradation rates of the IONPs remain unknown.

IONPs that are carefully synthesized to stealthily pass the Kupffer cells, usually have longer circulation time but may have greater uptake by phagocytic cells of MPS organs other than liver. For example, Cole *et al.*[79] reported a higher uptake of the nanoparticles in spleen compared to liver, after addition of a polyethylene glycol (PEG) layer around the cross-linked starch-coated IONPs. The exact mechanism of such selective uptake of these IONPs by spleen macrophages is still unknown. The authors reported two possible scenarios for this observation: first, PEGylation reduced the uptake by liver Kupffer cells, increased the half-life from 7.29 h to 11.75 h, and therefore macrophages in spleen had more time to remove the IONPs from the blood. Second, the higher spleen uptake might be due to increase of the hydrodynamic size of the IONPs to values larger than 200 nm after injection, because of plasma proteins adsorption or possible aggregation. The critical role of the hydrodynamic size on liver and spleen uptake will be discussed later in Section 2.1.4.

Recent reports also demonstrate that either nanoparticles or monocyte–macrophages can be selectively manipulated to facilitate their phagocytosis and targeting abilities.[80,81] For instance by either specific coating of nanoparticles (*e.g.* IgG coated IONPs[80]) or by pre-treating phagocytic cells with specific cytokines[81] the phagocytic and tissue or lesion homing capabilities of particle containing phagocytes can be influenced. These approaches can potentially enable nanoparticle containing monocytes or macrophages to be targeted to sites of infection, inflammation or neoplasia for therapeutic or imaging purposes.[82]

It is also possible to manipulate the immune system of the body to prolong the circulation time of the IONPs. For example, reducing the number of active Kupffer cells by pre-injection of another material, such as liposome particles coated with a chelated Ni^{2+} layer. Ni^{2+} has a higher affinity to adsorb the plasma protein through opsonization and therefore it has a high rate of initial macrophage uptake. The IONPs injected after this pre-treatment step showed a prolonged half-life up to 5 times more than the IONPs directly injected without administration of decoy liposome particles.[83] However, for further clinical applications of this approach, it is also necessary to evaluate the long-term toxicity of these decoy particles, in addition to all other concerns related to safety of the IONPs. As an alternative approach, Wang *et al.*[84] labeled red blood cells with IONPs and observed a significantly longer blood circulation time and efficient tumor targeting after intravenous administration of these cells.

It is important to note that macrophage uptake of the IONPs can have either beneficial or detrimental effects, based on the desired application.[85] For example, for targeting cancers in various tissues,[86] or identifying metastatic cancers in the lymph nodes,[87,88] and vascular angiography,[89,90] longer circulation time as a result of lower macrophage uptake is desired. On the other hand, for some other imaging applications such as evaluation of brain lesions,[91–93] assessment of rejection of the transplants or grafts,[94] visualization of heart plaques[47,95] and

various other inflammation-mediated diseases[27,96–98] higher uptake rates of the injected IONPs by specific macrophages (other than the Kupffer cells) or circulating monocytes and their subsequent homing to specific tissues is desired.

Liver. Liver blood vessels contain highly fenestrated sinusoids, with a certain average pore size of 100–200 nm (depending on the animal or human species), lined by Kupffer cells (Fig. 2).[100,101] As described earlier, Kupffer cells are the most effective macrophages to quickly phagocytize the nearby IONPs from the blood.[102] Liver uptake of IONPs has been reported as the most effective elimination pathway of the nanoparticles, even when the IONPs are tuned for specific targeting of tissues or organs (*e.g.* tumors).[58] Due to the high rate of IONPs accumulation in the liver,[103] the organ can be easily imaged using the IONPs as T_2 contrast enhancement agents in MRI or as tracers for the newly emerging technique of magnetic particle imaging (MPI).[65] In particular, this is helpful in MR imaging of potential liver cancers, since the IONPs that are taken up by the Kupffer cells in the healthy liver generate a dark contrast in T_2-weighted MRI and the tumor sites, lacking Kupffer cells and thus phagocytized IONPs, appear as bright regions.[104,105]

Hepatocytes are physically separated from the sinusoids by a region called the space of Disse (Fig. 2).[106] As discussed in Section 3.1, hepatocytes also accumulate the biodegradation byproducts of IONPs in the form of a protein–iron complex, called ferritin. Although the Kupffer cells found in the sinusoids are normally the main entrapment sites,[107] if suitably functionalized, IONPs can also accumulate in hepatocytes.[108] Hepatocyte delivery of the IONPs can be enhanced by addition of molecules with high hepatocyte binding affinities (*e.g.* linoleic acid[109] and lactobionic acid[110]) to the surface of the IONPs, or by increasing the percentage of antifouling molecules such as PEG[106] on the surface of the IONPs to decrease their rate of opsonization.

Accurate mapping of the distribution of IONPs in the liver demands detailed experimental studies. For example, Van Beers *et al.*[111] used different imaging techniques to study the distribution of ultrasmall dextran coated IONPs (Ferumoxtran, core size, $d_C \sim 5$ nm, $d_H \sim 30$–35 nm) in the liver using a rat model. They used chemical staining of the ferric ions (Fe^{3+}), in liver sections and showed by light microscopy analyses that maximum uptake of the IONPs (injection dose of 15 μmol Fe kg^{-1}) by the Kupffer cells occurred after 1–4 hours of injection. This peak was delayed to 8–24 hours when the dosage was increased to 150 μmol Fe kg^{-1}. MR images on the other hand, showed a change in liver contrast, 1 hour after injection of the higher dosage (150 μmol Fe kg^{-1}), suggesting IONPs were still distributed in the extracellular blood and interstitum, rather than Kupffer cells or hepatocytes. Closer inspection using electron microscopy analysis in ultrathin sections of the liver showed only sparse IONP uptake in the hepatocytes after 24 hours of administering the higher dosage (150 μmol Fe kg^{-1}).

Spleen. Macrophages residing in the reticular meshwork of the spleen and bone marrow also act as efficient filters for removing the IONPs from the bloodstream. For example, an artery entering the splenic pulp terminates in small, highly porous capillaries that allow the blood to enter into the marginal and red pulp zones and then get squeezed into collecting veins through the fenestrated venules in the red pulp regions (Fig. 3).[112] The macrophages present in marginal and red pulp zones of the spleen phagocytize the IONPs.[113] Studies on rats and mice have shown the presence of the IONPs either in the red pulp or particularly in the marginal zones around the white pulp regions of the spleen.[65,114] The filtered blood then passes through the endothelial walls of the venous sinusoids and finally returns to circulation. Macrophages lining these venous sinuses also act as the secondary filtering barrier for the IONPs.[112]

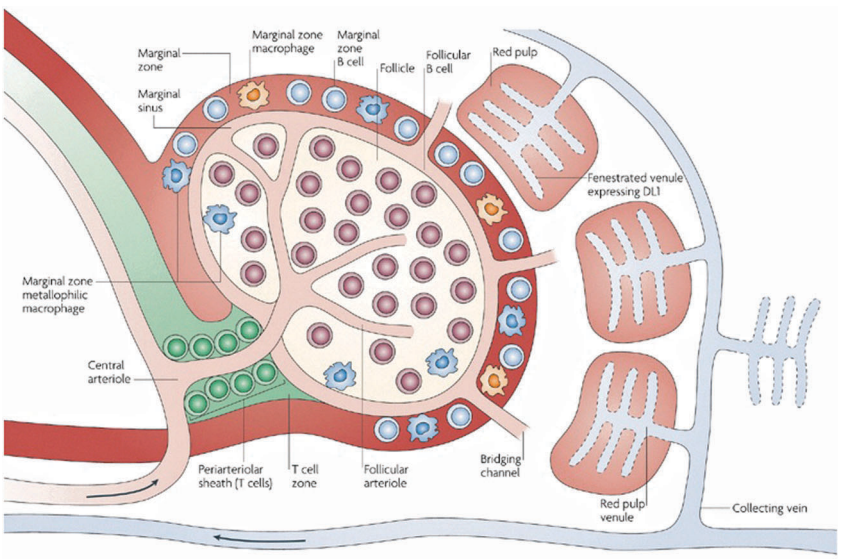

Fig. 3 The spleen microstructural anatomy and pathway of the IONPs entering the spleen through its central arteriole. This artery terminates in highly porous small capillaries that direct the IONP into the marginal zones around the white pulp where macrophages actively take up the nanoparticles. Re-printed with permission from ref. 115. Copyright 2009, Nature Publishing Group.

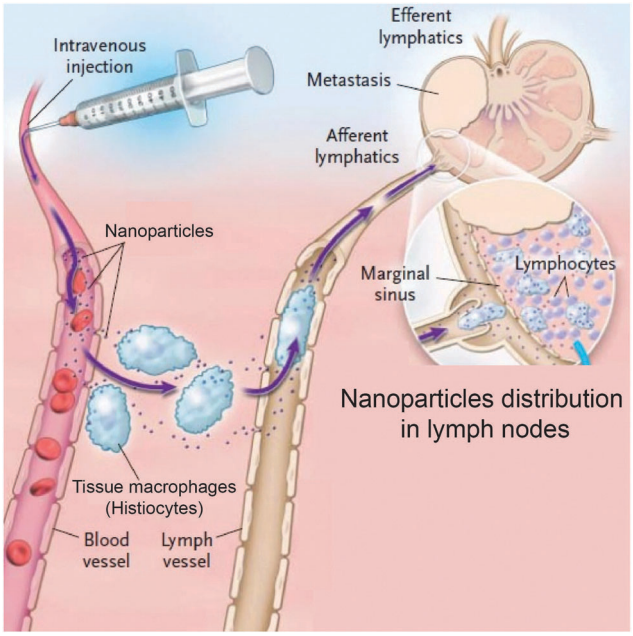

Fig. 4 Pathway of the IONPs in lymph node system. IONPs get taken up from the blood vessel by the lymph node macrophages (histiocytes) and then get shuttled to the lymph vessel through afferent lymphatics. Adapted with permission from ref. 117. Copyright 2003, Massachusetts Medical Society.

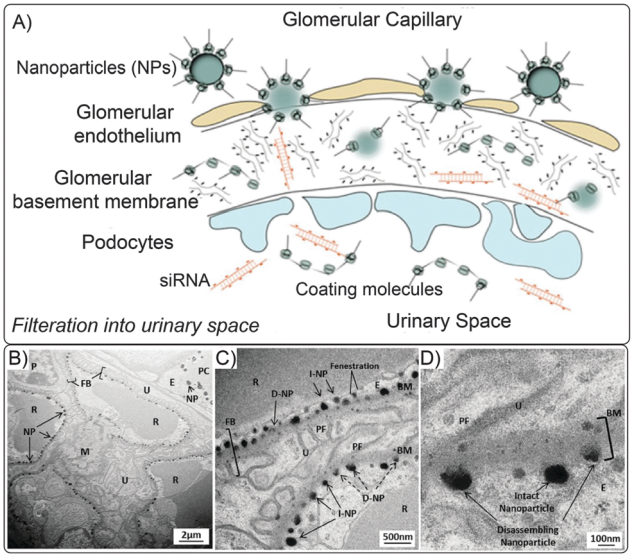

Fig. 5 (A) Excretion pathway of the IONPs or their degradation products through kidney. IONPs enter the glomerular capillaries through the afferent arterioles. IONPs smaller than 10–15 nm, their detached coating molecules, therapeutic agents (*e.g.* siRNA) or degradation bi-products present in the blood can pass the glomerular endothelium and fenestrations between the podocytes, where they actually get transferred to renal tubules and are excreted in the urine *via* the bladder. Transmission electron microscopy (TEM) images in parts (B)–(D) show that nanoparticles (NP) were trapped in these fenestrae due to their large sizes (~60–100 nm). (BM: basement membrane; FB: filtration barrier, (I/D)-NP: (intact/disassembling) nanoparticle; P: podoyctes; U: urinary space; PF: podocyte foot process; M: mesangium, PC: peritubule capillary; E: endothelial cell; R: erythrocyte). Re-printed with permission from ref. 125. Copyright 2012, National Academy of Sciences.

Lymph nodes. Lymph nodes are widely distributed in the body and linked together by a network of lymphatic vessels. If IONPs enter a tissue, they ultimately may enter the lymph surrounding that tissue.[112] They, then get directed to the regional lymph nodes by way of afferent lymphatics and get trapped in the sinusoidal reticular meshwork lined with macrophages.[116–118] The IONPs in tissues may also be phagocytized by histiocytes present in the interstitum. These histiocytes then migrate to the lymph nodes through lymph vessels as shown in Fig. 4.[116,117] The filtered lymph passes out of the node through efferent lymphatic vessels and finally reaches the venous blood.[118] The major fraction of the IV injected IONPs usually get filtered first by the liver and spleen, before reaching any other organs and their surrounding lymph nodes. An exception would be IONPs that are injected intramuscularly or subcutaneously. In these cases regional lymph nodes may be the initial filter point.

2.1.3 Renal clearance: a non-phagocytizing pathway. Nephrons are the major functional and structural units of the kidney and each kidney has over a million nephrons. They help the kidneys maintain the homeostasis of body fluids and electrolytes among intracellular, extracellular, and extravascular compartments. They are also responsible for selective filtering of carbohydrates and proteins from the blood, as well as ions and even nanoparticles with $d_H < 10$–15 nm, if present. The generally agreed size range constraints for clearance of the nanoparticles through kidneys and other organs (*e.g.* liver and spleen)[10,119,120] will be discussed in detail in Section 2.1.4.

The intravenously injected IONPs enter the blood vessels of the nephrons through the renal hilum and are eventually excreted in urine *via* the ureter, then *via* the urinary bladder. However, first they must pass through the glomerulus. During this clearance pathway, the IONPs or their degradation products, first reach the glomerular capillaries – the blood filtration sites in the nephrons – through afferent arterioles and the filtered blood leaves the glomeruli through efferent arterioles. The elements for excretion that are filtered from the blood, (ultrafiltrates), enter Bowman's space after passing through gaps between the podocytes forming the glomerular basement layer of the capsules (Fig. 5).[121] These intercellular filtering slits are also referred to as fenestrae. Note that the filtration mechanism in the kidney is physically different from the mechanisms in liver and spleen. The kidney fenestrae act as filters that only allow species smaller than a certain size ($d_H \sim$ 10–15 nm) to leave the bloodstream and get excreted from the body, but liver and spleen sinusoids act as filters that entrap blood borne elements larger than a certain size (see Section 2.1.4). The hydrodynamics of the blood pressure, flow and viscosity and the filterable elements size and charge determine the filtering efficiency of the nephrons.[122] In addition, the number and size of these channels is controlled by physiological and pathological conditions and varies from species to species. Eventually, the ultrafiltrate solution containing any IONPs reaches the renal pelvis, where they get transferred to the urinary bladder *via* the ureters.

If renal clearance is the appropriate clearance route for a specific type of IONPs, a large percentage of the administrated IONPs dosage should be excreted through urine.[119] However, due to size constraints, no specific reports describe the presence of the non-degraded IONPs in urine.[123] However, small coating molecules that are detached from the surface of the IONPs due to their weak bonding and other small biodegradation byproducts may be excreted through kidney (Fig. 5).[124,125]

Note that labeling of IONPs by coating molecules (*e.g.* by fluorescent molecules) is not necessarily a reliable approach to prove the presence of the IONPs in urine, since in most of the cases the coating materials can get degraded and independently be cleared out of the body through the kidneys much faster than the iron oxide core of the IONPs.[126,127] When IONPs coating molecules are labeled with fluorophores, it is possible to study the co-localization of the IONPs and their coatings in tissue sections by confirming the presence of blue foci generated by the Prussian Blue staining of the iron in the core and the fluorescent signal from the coating of the IONPs at the same location in tissues.[56] Even though there are some reports of the accumulation of the IONPs in kidney,[128,129] the critical evidence for renal clearance, *i.e.* traces of IONPs in urine, were not presented in these studies. The observed MRI or fluorescent contrast enhancements in the kidney might be only due to the presence of the blood circulating IONPs or their micron size aggregates in the efferent and afferent blood in the capillaries and arterioles in the renal cortex and not necessarily from the glomerular uptake.[56,79,130,131]

2.1.4 Parameters determining the blood clearance pharmacokinetics

Hydrodynamic size and stability of the IONPs. Hydrodynamic size of the IONPs is one of the most important factors that determines their biodistribution kinetics.[132] The effect of hydrodynamic size, d_H, on the pharmacokinetics of polymer and gold nanoparticles have been discussed at length,[9,119,120,133,134] and it is reasonable to expect similar behavior for IONPs as well. A recent study has clearly shown the decrease of the blood half-life of IONPs from 50 to 3 minutes by increasing their hydrodynamic size from 20 to 85 nm.[135] As shown in Fig. 6, IONPs with $d_H > 100$ nm quickly accumulate in the liver and spleen through macrophage phagocytosis and entrapment in liver and spleen sinusoids (Section 2.1.2).[58,136] In addition, it has been reported that IONPs with $d_H > 200$ nm have higher rates of uptake by the spleen when compared with the liver, due to their mechanical filtration followed by macrophage phagocytosis in spleen.[79,137,138] Pinocytosis (a mechanism for cellular uptake of the smaller nanoparticles occurring by a non-specific and non-receptor mediated cell membrane absorption) by liver and spleen macrophages has been reported as the main internalization pathway for dextran-coated IONPs with $d_H < 20$ nm.[139,140] Larger IONPs can get internalized through receptor-dependent endocytosis.[139] In both cases, the internalized IONPs get transferred to lysosomes. Finally, it is highly likely that IONPs with d_H, <10–15 nm[73,119] are eliminated *via* the kidneys according to the mechanisms discussed earlier in Section 2.1.3 (Fig. 6). Due to variation in IONPs characteristics and experimental parameters (such as

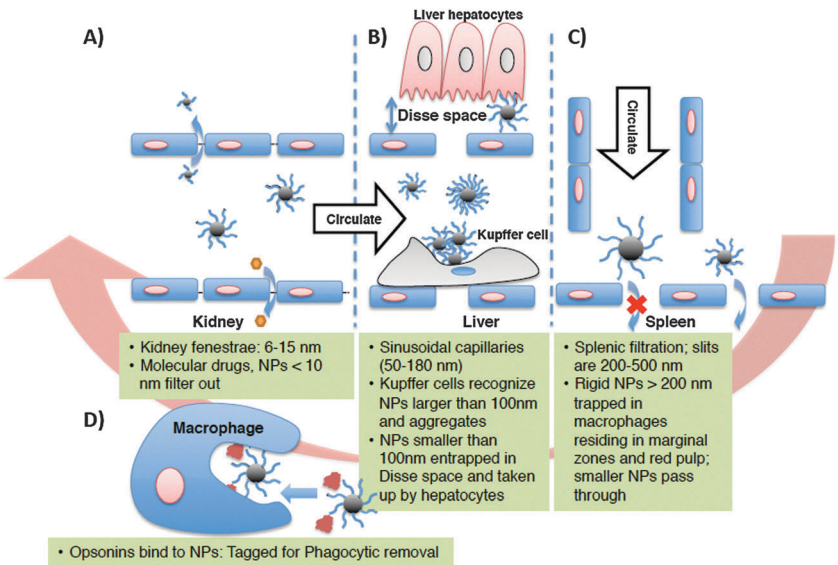

Fig. 6 Schematic showing the size dependent physiological barriers against nanoparticles blood circulation. (A) In human kidneys, nanoparticles with $d_H < 15$ nm in diameter are filtered out, thus imposing a lower size limit for designing long circulating nanoparticles. (B) Sinusoidal capillaries in the liver are fenestrated (50–180 nm) and lined with the Kupffer cells, which rapidly uptake large nanoparticles or agglomerates tagged with opsonins, and smaller nanoparticles are trapped in the Disse space and can be taken up by hepatocytes. Meanwhile, nanoparticles <100 nm in diameter with non-fouling (prevent protein adsorption) and non-immunogenic (prevent immune response) coatings continue circulating. (C) The spleen imposes the true upper limit in optimal size for circulation – nanoparticles larger than about 200 nm get trapped in the marginal zones and red pulp, where they are sequestered by the splenic macrophages. (D) Finally, opsonization is the tagging of nanoparticles with specialized proteins called opsonins for removal by phagocytic cells of mononuclear phagocytic system (MPS), which includes the Kupffer cells in the liver and the splenic macrophages in the marginal zones and red pulp.

animal models, quantification techniques *etc.*) used in different studies, the exact upper and lower size limits to avoid or enhance hepatic and renal clearance are not well-defined, but the range of sizes provided here are the most agreed upon values for each of the IONPs elimination mechanism discussed above.[13]

Blood half-lives of different types of IONPs with a wide range of hydrodynamic sizes are briefly listed in Table 1. Generally, MPS elimination of the IONPs is the dominant mechanism since the hydrodynamic size of the IONPs are usually larger than the size limits for renal elimination.[141] Therefore, as a simple rule of thumb, by tuning the hydrodynamic diameter of the IONPs between approximately 10–100 nm, it is possible to extend their blood half-life and increase the access of the IONPs to other organs such as lymph nodes,[142,143] arterial walls,[58] brain[144] or tumors.[2] However, it is important to note that even if d_H = 10–100 nm on average, there may be some fraction of the IONPs (or their aggregates) with sizes beyond this range. The percentage of these fractions depends on the distribution, or the polydispersity index (PDI) of the hydrodynamic size of the IONPs, which is typically determined in solution using dynamic light scattering (DLS). PDI is a dimensionless number, usually ranging from 0.05 to 0.7 and describing the amount of non-uniformity of nanoparticles hydrodynamic size distribution. PDI values smaller than 0.05 are rarely seen, only for highly monodisperse standards and values greater than 0.7 show that the nanoparticles are highly polydisperse, having a very broad hydrodynamic size distribution. A high PDI indicates a broad distribution of nanoparticle diameters, which results in their multi-stage clearance since larger nanoparticles circulate for shorter periods compared to smaller IONPs.[145] For instance, Briley-Saebo *et al.*[40] used filtration to fractionate Feridex (d_H = 121 nm, with polydispersity index, PDI, of 0.4) IONPs based on their size and only used the smaller size (d_H = 15 nm, PDI = 0.2) portion of the original batch for biodistribution studies. They found that fractionation of Feridex increased the blood half-life in mice from 0.46 h to 15.9 h and decreased the liver accumulation dosage from 60% of the injected dose to only 6.4% after 44 h post-injection. In general, the lowest possible PDI is preferred in order to get more reliable and repeatable *in vivo* blood clearance pharmacokinetics and subsequent biodistribution results.

Size instability caused by aggregation of the injected IONPs also plays a detrimental role in their clearance kinetics.[16] When the injected IONPs are not stable in the blood, they form aggregates to decrease their surface energy, which results in their rapid entrapment by the MPS system. IONPs aggregates can form due to various reasons; for example, they form when the steric hindrance or electrostatic repulsion forces between the individual IONPs are not strong enough to prevent the nanoparticles from forming these clusters.[146] Alternatively, when the coating molecules are weakly bound to the IONP cores, they are easily detached in the presence of highly ionic species in the surrounding biological media, resulting in IONP aggregation.[147] Usually, in these cases, cross-linking of the coating molecules can improve the IONPs stability and blood half-life.[15,52] Adsorption of plasma proteins on the IONPs can also increase the size and MPS elimination rate of the IONPs.[148] Therefore, by utilization of a proper surface modification approach (see Coating molecules section below), both stability and circulation time of the IONPs can be improved.[149]

Core size. Biomedical IONPs are usually made of crystalline iron oxide cores with superparamagnetic properties.[1] Core size, d_C, of the iron oxide nanoparticles plays a very important role in determining their saturation magnetization and dictates their T_2, T_2* and T_1 relaxation times when used as MRI contrast agents.[19,150,151] For example, increasing d_C of IONPs from 5 to 14 nm, increases T_2 relaxation rate of the surrounding protons (r_2 relaxivity) by a factor of three.[152] In the recently developed biomedical imaging technique, called magnetic particle imaging (MPI), IONPs behave as tracers – unlike MRI, where the IONPs simply alter contrast of surrounding tissue, IONPs in MPI are the source of the imaging signal – and larger crystallite sizes ($d_C \sim$ 23–27 nm) generate images with higher resolution and brightness.[18,153] However, faster biodegradation rates in liver and spleen has been recently reported for monodisperse 5 nm iron oxide cores in comparison with 15 and 30 nm IONPs and coated with the same coating molecules.[107] This may raise long-term toxicity issues for larger core sizes, because of a longer dwell time.

In an ideal surface modification process that results in a uniform coating thickness with the same type of molecules, larger core sizes should result in larger hydrodynamic sizes. However, larger crystal sizes have strong magnetostatic or dipolar interactions with each other, which often results in the formation of clusters of the cores with larger hydrodynamic sizes. This also makes their surface modification more challenging. As discussed in the previous section, for larger hydrodynamic sizes, especially when $d_H > 200$ nm, a shorter half-life is expected due to the rapid hepatic and splenic filtration of the nanoparticles. Also, for a constant iron dosage, the total surface area is less for larger core sizes, which mean less chemically or physically active sites are available for conjugation or loading of the desired polymer coatings and therapeutic biomolecules on the IONPs.[154] Therefore, there is always a competing role between higher imaging efficiency and longer blood residence time with accompanying therapeutic performance of these larger contrast agents both in MPI and a wide range of T_2 MRI applications.

For example, as shown in Table 2, r_2 relaxivity of the ultrasmall IONPs (LUSPIO) with smaller core ($d_C \sim$ 2–5 nm) and hydrodynamic ($d_H \sim$ 10 nm) sizes was about one third of LSPIO nanoparticles, ($d_C \sim$ 7–12 and $d_H \sim$ 35 nm).[58] However, the blood half-life of LUSPIO was $\sim$1.5 times more and its liver accumulation was 30% lower than the LSPIO nanoparticles. When different antibodies were conjugated to these IONPs for targeting of heart lesions, the blood half-life of the LUSPIO was again 30% more and the liver uptake was about 10–15% less than LSPIO. Note that smaller IONPs have a higher r_1 (the T_1 relaxation rate of the water protons surrounding each nanoparticle) and are thus often used as contrast agents, which provide brighter images in T_1-weighted MRI.[19] A longer circulation time is generally expected due to their smaller sizes, but

Table 2 Effect of hydrodynamic size of the IONPs on their r_1 and r_2 relaxivities in MRI, their blood half-lives in normal and wild type mice and dosage percentage accumulated in the liver. The hydrodynamic sizes were based on number percentage average and the injection dose (ID) was 3.9 mg Fe kg^{-1} body weight. ($ApoE^{-/-}$: apolipoprotein E deficient: WT: wild type mice; IK17: human antibody; LSPIO: lipid-coated superparamagnetic iron oxide particle; LUSPIO: lipid-coated ultra-small superparamagnetic iron particle; MDA2 and E06: murine antibodies.) Re-printed with permission from ref. 58. Copyright 2011, Elsevier B. V.

Formulation	Size (nm)	r_1 (s^{-1} mmol l^{-1})	r_2 (s^{-1} mmol l^{-1})	Blood half-life $ApoE^{-/-}$ (h)	Blood half-life WT (h)	%ID in liver (24 h p.l.)
Untargeted LUSPIO	10 ± 3	14 ± 1	35 ± 2	1.52	1.41	25
Untargeted LSPIO	35 ± 5	12 ± 1	103 ± 4	1.02	1.01	35
MDA2 LUSPIO	14 ± 3	13 ± 1	37 ± 2	9.01	1.55	31
MDA2 LSPIO	38 ± 4	11 ± 1	117 ± 5	7.28	1.12	37
IK17 LUSPIO	12 ± 2	14 ± 1	35 ± 2	9.12		31
IK17 LSPIO	36 ± 4	10 ± 1	106 ± 5	7.30		34
E06 LUSPIO	16 ± 4	12 ± 1	38 ± 2	9.32		30
E06 LSPIO	39 ± 5	11 ± 1	119 ± 6	7.42		35

more systematic studies are needed to evaluate their short-term and long-term size-dependent biodistribution.[132]

In addition to size, monodispersity and shape uniformity of the iron oxide cores – important parameters often tuned to improve the imaging performance of the IONPs – may also affect their biodistribution and pharmacokinetics. Controlled high temperature decomposition of iron organometallics (*e.g.* iron pentacarbonyl and iron oleate) results in highly uniform and monodisperse IONPs.[155,156] However, these IONPs are coated with hydrophobic surfactant molecules (*e.g.* oleic acid and oleyl amine) and complex surface modification processes are usually needed to transfer them to aqueous media. Due to limitations of the phase transfer approaches, these IONPs have not shown a significant improved circulation time yet, specially compared with IONPs prepared by conventional co-precipitation in the presence of polymers such as dextran (Table 1).

Core morphology. Generally, one-dimensional nanostructures such as polymer filaments,[157] carbon nanotubes[158] and gold nanorods[159] with a high length to width aspect ratio have shown longer blood circulation times over the spherical counterparts.[160] The longer circulation time of one-dimensional nanoparticles has been attributed to lesser uptake by macrophages due to an opsonin-independent phagocytosis phenomenon.[159] The same trend is expected for iron oxide nanostructures with high aspect ratios.[11] For example, a prolonged blood half-life of up to 19 h has been reported for iron oxide "nanoworms" with longitudinal size of 70 nm, comprising a linearly aligned set of IONPs (~25 nm) encapsulated in dextran-PEG copolymer.[50] However, the largest fraction of the injected nanoworms accumulated in the lymph nodes (~40%), followed by the spleen (~15%) and liver (~9%).[161] This is in contrast to the more frequently reported results for spherical IONPs, in which liver has the highest uptake rate among the other MPS organs. Other recent studies[162,163] indicate that more systematic comparative analyses are needed to identify the exact clearance mechanisms and the optimum aspect ratios that enhance the blood half-life and pharmacokinetic performance of one-dimensional nanoparticles. It is also important to note that, experimentally, it is a difficult fabrication process to maintain all the other parameters (such as number of coating molecules, polydispersity and stability) effectively the same, and only change the core morphology and compare the pharmacokinetics and biodistribution results.[16,164] Such studies are even more complex when hybrids of iron oxide with other materials such as gold, carbon nanotubes, quantum dots, gadolinium or silica are used for *in vivo* investigations.[113,129,165–173]

Other IONPs morphologies such as cubes have also been used for *in vivo* studies, but the effects of these specific shape on their pharmacokinetics and biodistribution mechanisms are still unknown.[174] A recent study has shown that iron oxide nanocubes tend to form aggregates in the endosomes of the liver and spleen macrophages at the earlier stages of uptake, which decreases their endosomal degradation rate.[175] When shuttled from endosomes to lysosomes, the lysosome enzymes and proteins redispersed the aggregated nanocubes and subsequently increased their degradation rate.[175] TEM analyses showed that degradation happens faster at edges of these cubes (along (220) lattice planes), which are thermodynamically less stable crystallographic sites (Fig. 7).[175]

Coating molecules. Un-coated IONPs are often colloidally unstable, form aggregates and get eliminated by the MPS system quickly. The biodegredation rate of these aggregates is slower than the individual IONPs and can cause serious long-term safety issues, as discussed in Section 5.[175] There are some recent methods reported for developing colloidally stable un-coated IONPs.[176–179] However, further studies are required to evaluate the *in vivo* performance of these IONPs formulations. Different types of natural (*e.g.* dextran,[41] chitosan,[4] starch,[16,79] human serum albumin (HSA)[180] and phospholipids or liposomes[181,182]) and synthetic polymers (PEG,[107] Pluronic,[183] and different types of co-polymers[127]) have been used to improve the blood circulation time of the IONPs. Table 1 lists some of the most commonly used types of coating materials and the blood half-life of the corresponding IONPs. All these polymers and their prospective alternates are relatively non-toxic.[151]

Among these different types of the polymers, PEG has been the most popular coating option. It stabilizes IONPs primarily *via* steric hindrance, and has excellent anti-fouling characteristics (resists interaction with blood and serum proteins and therefore, reduces opsonization, macrophage uptake and subsequent MPS clearance of the IONPs).[99] Multiple mechanisms have been

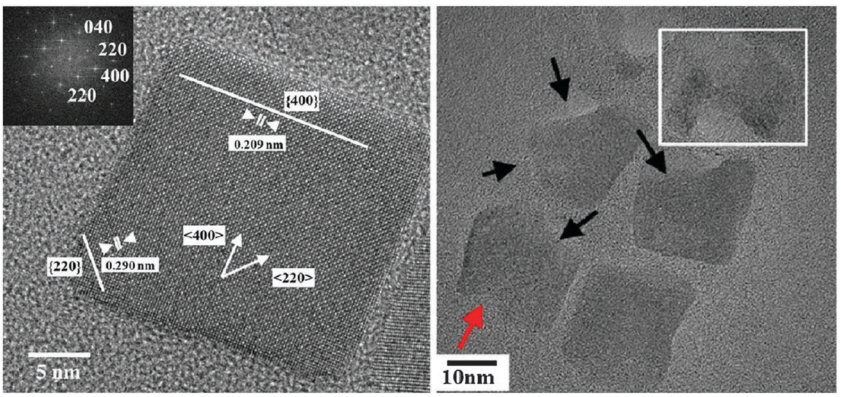

Fig. 7 Single crystalline iron oxide nanocubes (left) and their biodegradation in crystallographic directions with higher atomic surface energies after incubation in lysosome-like solution (right). Adapted with permission from ref. 175. Copyright 2013, American Chemical Society.

proposed in the literature regarding the stealth behavior of the PEGylated IONPs; the most accepted one is based on the shielding of the surface charge of the IONPs and increasing their hydrophilicity, which results in their reduced interactions with opsonin proteins.[184] For a wide range of therapeutic applications, it is desirable to combine the stealth characteristics of PEG with the novel functionalities of other polymers that enable conjugation of drugs or targeting molecules,[56] or sensitivity to pH and temperature changes in the surrounding environment.[185,186] Table 1 shows some examples of PEG-grafted-polymers that have been used for this purpose.

Although PEG is still the best candidate for coating of IONPs, there are some recent studies showing some possible drawbacks regarding its role in the enhancement of the nanoparticles pharmacokinetics when multiple injections are required (*e.g.* multiple IONPs administration is required to monitor tumor sizes over a specific period); specifically, the pharmacokinetics of the nanoparticles can be different with repeated injections. For instance, a very high rate of MPS uptake has been reported for some types of PEGylated IONPs in their second run of injection.[187] This phenomenon is called accelerated blood clearance (ABC) and its mechanism is not well understood.[188] A suggested mechanism is that anti-PEG IgM antibodies form in the spleen after the first IONPs injection, which remain in the blood and bind to PEGylated IONPs administered through subsequent injections; as a result, their uptake by Kupffer cells in the liver is enhanced.[189,190] ABC not only decreases the therapeutic performance of the IONPs by reducing half-life, but also raises serious concerns regarding the potential for liver damage, especially when IONPs act as carriers for highly toxic anticancer drugs.[191,192] Zwitterionic (or dipolar) materials such as dopamine sulfonate[193] and poly(amino acids),[194] polymers with heteroatoms in the main chain (polyglycerol[128]) and vinyl polymers (poly(vinylpyrrolidone)[104,195]) have been introduced as the best alternative materials for PEG.[196] The preliminary results show that nanoparticles coated with these novel polymers can have a long circulation time in blood.[197] However, the occurrence of ABC phenomenon for repeated administration of these novel polymers is still unknown.

The molecular weight, shape, charge and grafting density of the coating molecules on the surface of individual IONPs can also change the pharmacokinetic performance of the IONP.[16,106,164] For example, increasing the molecular weight of the PEG molecules enhances the stealth characteristics of the IONPs by covering a larger surface area of the IONPs, which results in their slower elimination and degradation by MPS macrophages.[16,79] Also, when the distance between the attachment sites of the coating molecules

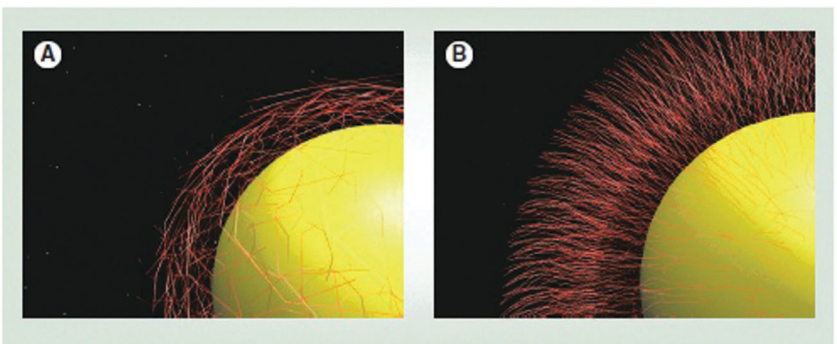

Fig. 8 (A) Mushroom-like configuration of the coating molecules on the surface of the IONPs which results in a lower density of the coating molecules and (B) brush-type assembly of the coating molecules which provides a high density coating layer. Re-printed with permission from ref. 99. Copyright 2011, Future Medicine.

to the IONPs surface is large (low surface density), a ''mushroom-like'' coating forms, with a shorter half-life in comparison with the ''brush-like'' conformation observed in high surface density coatings (Fig. 8).[99,198,199] This is due to better shielding of the IONPs surface against the opsonin proteins, provided by the denser brush like coatings.[184,200,201] The effect of charge on IONPs circulation will be discussed in the next section.

Some coating polymers such as PEG have highly flexible chains, with a large number of possible conformations. This makes a conformational ''cloud'' around the IONPs.[196] Statistically, when the rate of the transition of the coating molecules between their different conformations is high, the probability of the interaction of the plasma proteins with the IONPs is reduced and the blood half-life of the IONPs is longer.[202] The flexibility and stiffness of these polymers depends on their molecular structure parameters, such as size of the side groups and presence of polar groups or side chains in their backbone.[203] Polymers with higher glass transition temperatures (T_g) usually have higher rigidity.[204] Thermogravimetric (TG) studies are the standard way to determine T_g of the different polymers. More systematic studies are needed to identify exactly the role of these parameters on pharmacokinetics of the IONPs.[119]

The uniformity of the molecular weight of the polymer used for functionalizing the IONPs can also be an effective parameter for determining the circulation time of individual IONPs. For example, natural polymers such as chitosan and dextran usually have higher molecular weight polydispersity index (PDI) compared to synthetic polymers prepared by controlled chemical routes such as reversible addition fragmentation chain transfer (RAFT) polymerization.[205] In terms of producing uniform biodistribution performance, a low PDI might be more desirable.

Circulation time of the IONPs usually decreases when additional biomolecules such as cancer targeting agents and drugs are conjugated to the surface of the IONPs.[50] Increasing the average number of these molecules on IONPs decreases the blood half-life and consequently the targeting ability of the IONPs.[50] This is due to the increase in the hydrodynamic size of the IONPs after loading of these targeting agents. Therefore, there should be an optimum number of these molecules required on each IONP in order to get the highest therapeutic performance. This variation depends directly on the type, size and charge of the targeting molecule.[50] A PEG linker between the IONPs surface and the targeting molecules increases their residence time in the blood stream, due to steric hindrance and anti-fouling characteristics of PEG molecules.[50,127]

Finally, the binding strength of coating molecules with IONP cores has an effect on circulation time. Coatings that form weak non-covalent bonding to IONPs are prone to detachment from the IONPs *in vivo* after injection;[27] as a result, a large fraction of these separated small molecules or their biodegradation by-products accumulate in the kidney and are cleared *via* urine, while the remaining IONPs get aggregated and are delivered to the liver.[125,127,196] Cross-linking of the coating molecules forms a hydrogel around the IONPs that protects them against opsonization and increases their blood half-life.[206] For example, dextran molecules have a weak interaction with the surface of the IONPs through the hydrogen bonds between the hydroxyl groups of the dextran moiety and surface oxide hydroxide groups.[207] When the dextran molecules are cross-linked with each other using 1-chloro-2,3-epoxypropane (or epichlorohydrin) as an alkylating cross-linker, the blood half-life of the IONPs is increased up to 12 h in mice.[50,208] Increasing the dextran cross-linking percentage decreases the protein adsorption and prolongs the blood circulation time of the IONPs.[52] The same effects were reported recently for IONPs coated with cross-linked starch.[16]

Surface charge and zeta potential. The surface charge of IONPs directly depends on the molecular structure of the coating materials. For example, a positive charge is expected for IONPs with a higher number of amine groups,[16,209] while hydroxyl, sulphate and carboxyl groups usually contribute to a negative charge on IONPs.[12,197] Since charge affects the degree of protein adsorption on IONP surface, the types of the functional groups present on the surface of the IONPs are important in determining the blood circulation time of the IONPs.[209] Unfortunately, there is only limited information available regarding the direct role of these functional groups on the pharmacokinetic and biodistribution of the IONPs.

Zeta potential (which is measured in units of mV) has been routinely used as a parameter for estimating the surface charge of the nanoparticles. However, it is important to note that this parameter is calculated from the electrophoretic mobility (speed of the IONPs in an electric field) of the IONPs and is not an accurate representative of the nanoparticles surface charge.[210] Therefore, it is possible to see similar zeta potential values for different batches of IONPs that are coated with different numbers of the charged species on their surface.[211] These different charge densities on the surface of the IONPs might change their electrostatic interactions with the surrounding proteins and cell membranes and alter the blood circulation pharmacokinetics.[212] Therefore, considerable care must be taken to comparatively interpret the pharmacokinetic behavior of the IONPs based only on their zeta potential values.

The blood half-life of some IONPs with neutral, positive or negative charges are shown in Table 1. It is generally agreed that IONPs with a neutral surface charge have a slower rate of MPS or renal elimination.[73,213,214] For example, for IONPs with the same size and coating type (*i.e.* dextran), the half-life of the neutral Ferumoxtran-10 (d_H = 35 nm) IONPs in human body was longer than that of anionic Ferumoxytol (d_H = 17–31 nm) IONPs (24–36 h *vs.* 10–14 h).[48,136] A much faster blood clearance is generally expected for positive charge IONPs in comparison with negative charge IONPs,[215] because positively charged IONPs have a higher affinity to adsorb plasma proteins[216] and bind to macrophage or other cell membranes.[217]

However, there are still some discrepancies about the exact role of zeta potential ranges on the MPS clearance rates in different studies. For example, some reports link higher liver uptake of the IONPs only to positive charged IONPs with d_H > 100 nm.[119] But, on the other hand, it is also reported that negatively charged USPIO (SHU555C, d_H = 21 nm) coated with

carboxydextran have a much higher uptake by macrophages as compared with non-ionic Ferumoxtran-10 (d_H = 20–50 nm) IONPs coated with unmodified dextran.[218] In another study, liver accumulation of different sizes of PVP-coated IONPs with zeta potentials ranging from +12–14 mV were compared with Feridex (d_H = 58 nm and −25 mV).[104] It was shown that liver uptake of the positively charged IONPs was less than Feridex with slightly more accumulation observed in the liver for PVP coated IONPs, with d_H = 118 nm. In a separate study, Sakulkhu *et al.*[216] reported an almost similar blood circulation time for negatively charged (zeta potential ∼ −6 mV) and neutral (zeta potential ∼ 1.5 mV) PVA coated IONPs, with respective hydrodynamic sizes of ∼38 and ∼28 nm. Also, Cole *et al.*[16] reported a half-life of up to 12 hours in rats for PEG-modified starch coated IONPs with a zeta potential of about +25 mV.

These apparently controversial conclusions might be due to the fact that blood clearance of the IONPs is a complex phenomenon depending on the combination of the various parameters discussed above, *i.e.* size, shape, charge and the nature and density of coating molecules. In fact, it is technically difficult to maintain all the other parameters the same and compare the biodistribution results based only on one parameter such as zeta potential.[9]

Proteins adsorption. As discussed in Section 2.1.2, opsonization is a process by which the IONPs get encased by plasma opsonin proteins, making them recognizable by macrophages (Fig. 1 and 6).[199] Opsonization is usually followed by receptor-mediated phagocytosis of the nanoparticles by these macrophages or other phagocytic cells.[219] In addition, surface protein accumulation usually increases the hydrodynamic size of the IONPs, which accelerates their hepatic clearance.[104,209]

Various parameters determine the thickness and composition of the plasma protein corona forming around IONPs.[220] For example, the type, functional groups (*e.g.* amines, carboxyls and *etc.*) and charge of the coating molecules can significantly change the composition of the protein corona forming around IONPs.[216,221] Also, the amount of the adsorbed proteins is enhanced by increasing the size and surface roughness of the nanoparticles.[222,223] Mahmoudi *et al.*[209] incubated different sizes of IONPs with fetal bovine serum (FBS) and analyzed the composition of the protein corona formed around the nanoparticles. They reported that the larger molecular weight fraction of the proteins showed higher adsorption onto the surface of the larger IONPs, and smaller proteins interacted more with smaller IONPs. This is because protein molecules have a different conformational arrangement on nanoparticle surfaces compared to flat surfaces of the same material – a phenomenon that depends on the curvature of the binding surface.[223] The relatively larger curvature of smaller size nanoparticles limits the binding of large protein molecules, thus decreasing the corona size.[224] Also, the physiochemical and mechanical characteristics of the coating molecules can significantly alter the rate of the protein adsorption by the IONPs.[151,225] Anti-fouling coatings (such as PEG[226] and zwitterionic materials[193]) help minimize interactions with opsonin proteins. This can be achieved by either shielding the surface charge, increasing the hydrophilicity or decreasing the interfacial surface tension of the IONPs.[184,223] Also, protein interactions with nanoparticles decrease when the coating molecules have a high vibrational mobility and flexibility.[184] Additionally, some coatings have a high affinity for adsorbing dysopsonin proteins that suppress the macrophage uptake.[184,220] Finally, it is still not clear whether adsorption of a specific type of protein or a combination thereof is the most critical factor for the rapid recognition of the IONPs by MPS macrophages.[119]

Depending on their net charge, plasma proteins bind either to the iron oxide core or the coating layer; for instance, differential proteomic studies of dextran coated IONPs incubated with different types of plasma proteins has shown that cationic plasma proteins such as histidine-proline rich glycoprotein (HPRG) and high molecular weight kininogen (HMWK) bind to anionic magnetite cores, while immunoglobulins (IgG) and mannan-binding lectins (MBL) bind to the cationic dextran coating.[41] The slightly anionic characteristic of the core crystals was due to partial dissociation of $Fe(OH)_3$ during the co-precipitation synthesis.[227,228] Simberg *et al.*[41] compared the half-life of the IONPs in knockout mice and wild type (WT) mice (without any genetic manipulation and with all proteins existing in blood plasma) to find which plasma proteins play the dominant role in opsonization and recognition of the IONPs by liver macrophages. They also measured the half-life of clodronate liposome nanoparticles in mice with impaired liver uptake as a control for circulation of IONPs. It was shown that these plasma proteins do not play a significant role in blood clearance of the IONPs (Fig. 9(A)). Liver Kupffer cells recognized the IONPs with the same rate, regardless of the specific type of adsorbed proteins present in plasma (Fig. 9(B)).[41] Also their results showed that the proteins present in plasma do not completely mask the surface of the dextran coating or iron oxide core, suggesting that the IONPs could be directly recognized by Kupffer cells, with minimal influence from the opsonin protein coating.

Similar studies were used to determine the role of protein adsorption on blood residence time of IONPs nanoworms, coated with a cross-linked dextran layer.[206] Cross-linking created a stealth hydrogel around the IONPs and increased their half-life in mice from less than 1 hour to about 10 hours. It has been assumed for more than a decade that the cross-linked layer forms a barrier around the IONPs, preventing the adsorption of the opsonin proteins and diminishing their recognition by MPS macrophages.[50,208] However, the results of this recent study showed that while cross-linking increased the half-life of the IONPs, it did not change the adsorption of the plasma proteins to the iron oxide core or coating layers. The longer circulation time of the cross-linked IONPs was attributed to the diminished binding rate of the anti-dextran antibody to the surface of the IONPs due to decreased number of surface hydroxyl groups after cross-linking. These two studies show that to prolong IONPs circulation time, it is not necessary to completely prevent proteins adsorption to the nanoparticles. More investigations are needed to show if these results are specifically related to

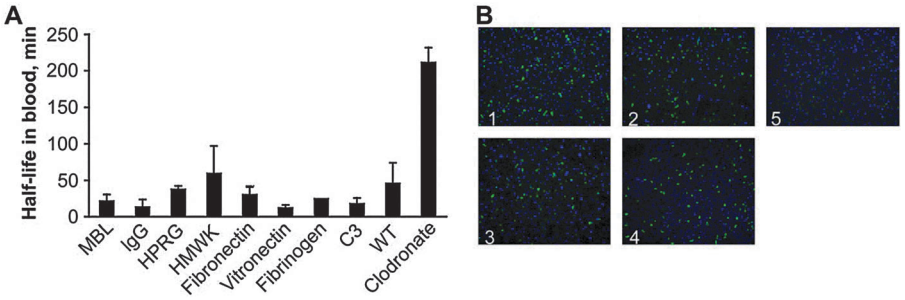

Fig. 9 (A) The half-lives of the dextran coated IONPs in different types of knockout mice (each lacking a specific plasma protein). The half-lives in various genetically engineered knockout mice (MBL, IgG, HPRG, HMWK, Fibronectin, Vitronectin, Fibrinogen and complement C3 deficient mice) were almost similar to their half-life in wild type (WT) control mice with all plasma proteins present in blood. Mice treated with clodronate liposomes had impaired liver phagocytic function which served as a control (right bar). (MBL: mannose-binding lectins; immunoglobulin G: IgG; HPRG: histidine-proline rich glycoprotein; HMWK: high molecular weight kininogen (HMWK)). (B) Histology of the liver sections confirm the results in part (A) and show that the Kupffer cells recognize and take up these IONPs (green dots due to presence of fluorescent molecules on their surface) regardless of the type of the proteins adsorbed to the surface of the nanoparticles after their injection. (Panel labels: 1, HMWK-deficient; 2, wild type; 3, complement C3-deficient; 4, MBL-deficient; 5, clodronate-treated mice). Re-printed with permission from ref. 41. Copyright 2009, Elsevier B. V.

dextran coated nanoworms studied in these reports or they can be generalized to other types of IONPs and coatings.

Technical factors. In addition to the characteristics of the IONPs described above, there are some important technical factors that can affect the circulation and pharmacokinetics of the IONPs. For example, the blood half-life of the IONPs is dose-dependent in both animal models[67] and humans.[55,229] An earlier study has shown that MPS elimination of the nanoparticles by macrophages in rat liver and spleen, gets saturated, when more than 10^{15} nanoparticles are injected.[230] The remaining nanoparticles usually circulate in the blood for longer times and have more chance to reach other organs.[67] A recent study in rodents has shown that the clearance rate of the nanoparticles is also dependent on the mice strain type and their particular immune systems.[81] Further, the circulation time usually increases with age, due to the reduced phagocytic activity.[60]

Except for a limited number of the iron oxide nanoparticles that are clinically approved (such as Ferumoxytol or Ferumoxide) or those that are undergoing clinical trials, most of the available half-life information of IONPs are limited to data derived from animal models. Therefore, it is important to know how to correlate the half-lives in different species for better prediction of IONPs circulation times in human patients. Usually, the blood half-lives in rodents are much shorter than in human due to faster heart rates and circulation time in rodent models (*e.g.* about 670, 420 and 75 beats per minute for mice, rats and human, respectively).[134] For example, the blood half-life of 45 μmol Fe kg^{-1} of AMI-227 IONPs is 24 h and 2 h in humans and rats, respectively.[231]

2.2 Pharmacokinetics and clearance of IONPs in other administration methods

Intrapulmonary delivery (inhalation or intratracheal instillation) of the IONPs is predominantly used for imaging and treatment of lung diseases.[232] IONPs administrated using the intranasal pathway eventually enter the alveoli spaces in the lungs.[233] In studies of mice, the inhaled IONPs mostly accumulated in the central lung region – about 2.5 times more than in the peripheral lung zones – without any considerable difference between the right and left lungs.[234] The respiratory innate immune system acts as the major barrier against their entrance into blood and other organs.[235,236] The macrophages that are present in the alveolar spaces phagocytize the IONPs, digest them and their by-products get released into the pulmonary lymphatics or they are swallowed.[237,238] A recent study has shown that the presence of the IONPs can increase the number of lung macrophages by the migration of monocytes into the lung, which enables faster ingestion of the IONPs.[239] The intranasal pathway is also known as a feasible way to deliver molecules to the brain.[240] However, the reported results related to IONPs are still controversial and the mechanisms for overcoming the BBB through this method are still unknown.[241–243]

The size, charge, coating and state of agglomeration of IONPs also play an important role in their clearance kinetics through the lung macrophages. Al Faraj *et al.*[235] instilled uncoated IONPs (d_C = 20–30 nm) *via* an intratracheal plastic catheter and showed that even 14 days after administration of the IONPs, about 88% of the dosage was still present in the lung but other organs were not different from control values (Table 3). The biodistribution of the injected IONPs was also presented in this table for comparison, showing that major part of the IV administrated IONPs were accumulated in the MPS organs. Cho *et al.*[236] used negatively charged cross-linked IONPs (d_H = 36 nm) after labeling them with fluorescent molecules (Cy5.5) and reported that major fraction of the IONPs were cleared from the lung 3 h after administration due to increased macrophage uptake in the lung. Using a fluorescent tag, they showed that the nanoparticles were mostly excreted in the urine in 24 h. Additional studies are required to confirm if these observed fluorescent signals in urine were from the degradation by-products or detachment of the coating molecules after administration of the IONPs or not. Also, the presence of any excreted magnetic iron oxide cores in urine

Table 3 Biodistribution of the IONPs administered through intratracheal instillation in comparison with intravenously (IV) injected IONPs and control mice instilled with saline. The instilled IONPs are mostly accumulated in the lung, while the IV injected IONPs are mainly entrapped in MPS system. Re-printed from ref. 235. Copyright 2008, Wiley-VCH Verlag GmbH & Co. KGa

Iron assay	Control (n = 2)	Instilled (n = 4)	Injected (n = 2)
Lung	67.9 ± 5.6	278.1 ± 6.8	93.5 ± 6.7
Liver	103.5 ± 30.4	104.6 ± 21.6	339.5
Spleen	347.9 ± 45.5	341.8 ± 64.7	492.3 ± 78.7
Kidneys	68.2 ± 9.5	59.7 ± 8.1	91.4 ± 12.3
Blood	384.8 ± 9.6	410.2 ± 61.4	487.8 ± 45.8
Brain	13.8 ± 0.9	17.6 ± 2	22.3 ± 4.5
Heart	91.9 ± 28.1	95.8 ± 20.6	96.1 ± 24.4
Thymus + LN	32.8 ± 11	35.0 ± 9.9	39.1 ± 9.4
Testicles	15.1 ± 1.4	14.2 ± 1.3	13.7 ± 1.8

Iron assay by ICP-OES in μg g^{-1} of organ in the follow-up study after sacrifice at day 14.

could be quantified by determination of any magnetic signal from the urine. Other studies by Kwon *et al.*[243,244] also showed that after 28 days of inhalation exposure to silica coated IONPs (d_H = 50 nm) a high percentage of the IONPs were accumulated in the liver, kidney and testis and the percentage of the IONPs remaining in the lung was similar to other tissues (*e.g.* brain, heart, spleen, *etc.*). Further studies are required to clarify the degradation mechanisms, clearance pharmacokinetics and exact biodistribution of the IONPs administered by this method.

Oral administration of the IONPs has been mainly used for MR imaging of the gastrointestinal (GI) tract. The IONPs used for this method are usually larger than the IONPs used for IV or inhalation.[245] For example, Ferumoxsil (AMI-121, coated by silica, d_H = 300 nm diameter) has been tested for pioneering clinical studies in the 1990's.[246,247] There are some major biological barriers against the successful GI delivery of the IONPs. For example, the gastric acids and enzymes can degrade the IONPs in a short time. However, proper coating materials (such as casein protein, silica and poly(lactide-*co*-glycolide acid)) with pK_a values lower than 3–5, helps to efficiently protect the nanoparticles against these active digestion mechanisms.[248–251] Here, pK_a is a constant parameter for each type of coating and is defined as a pH value above which the coating starts to dissociate.

Depending on the type of application, the IONPs that survive the acidic environment in the GI tract might need to pass the transport barrier of the intestinal epithelium. This can be achieved by using epithelial permeation enhancers such as peptides that can specifically bind to FcRn receptors in intestine epithelial layer.[252] Then, IONPs should pass through the liver sinusoids before entering the general blood circulation system. This means that most of the surviving IONPs might be taken up and eliminated by the Kupffer cells present in these sinusoids. In fact, the liver is again the major clearance organ in the pathway of these IONPs, unless special surface modifications have been used to enable stealthy behavior to resist phagocytosis by these macrophages. The IONPs remaining in the intestine are excreted through the feces, as reported recently by Smith *et al.*[253] The iron ions and detached or decomposed coating molecules, formed by digestion of the IONPs can also get shuttled to the portal blood or excreted from the GI track following the intestinal fluid flow.[254]

Other injection routes such as intra-peritoneal (IP),[255–257] retroorbital,[51,58] intravitreal (inner cavity of the eyes for intraocular drug delivery),[258,259] intra-muscular and subcutaneous injections have also been used as alternative methods for administration of the IONPs. Tsuchiya *et al.*[255] showed that intra-peritoneally injected IONPs mainly distributed in liver, lymph nodes and lung. Kim *et al.*[256] showed that IP injected IONPs can pass the blood–brain- and blood–testis-barriers in addition to usual accumulation in MPS organs. Biodistribution of the IONPs injected *via* the eye depends on their route of administration. For example, IONPs can enter into general blood circulation pool by retroorbital (as opposed to intraorbital) injection and reach other organs such as liver and targeted tissues.[51,58] However, no traces of the IONPs were observed in other organs after their intravitreal injection.[258,259] Nanoparticles administered by this method accumulated at corneal, retinal, scleral and optic nerves.[260] Intra-muscular and subcutaneous injections of the IONPs have been recently used for adjuvant-free malaria vaccine delivery[261] or non-invasive imaging of the sentinel lymph nodes to monitor breast cancer metastasis.[262,263] However, more studies are required to determine the long-term biodistribution and clearance of the IONPs injected by these methods.

2.3 Biodistribution of IONPs in other organs and tissues

Brain. The blood capillaries found in different locations of the body are formed from endothelial cells and the exchange of small molecules (such as gasses, inorganic ions, monosaccharides and amino acids) between the blood and interstitial fluids occurs through the gaps between these cells. In the brain, endothelial cells are tightly fused in the capillary walls, due to some contribution by astrocytes. This forms a minimally penetrable layer, known as the blood brain barrier (BBB), that protects the brain from some toxins, hydrophilic molecules and in general, against many infectious agents (Fig. 10). Gasses and other hydrophobic molecules such as transport facilitating peptides can pass this barrier by diffusion through the hydrophobic lipid bilayer membrane of the cells. These peptides facilitate the transport of hydrophilic molecules (*e.g.* carbohydrates and amino acids) through the BBB.

Unfortunately, the BBB also prevents the delivery to the brain of desired therapeutics such as drugs and nanoparticles needed for a wide range of tumor diagnosis and treatment trials; consequently requiring more direct and invasive administration methods such as intracranial injections.[264] In order to avoid such invasive administration routes, researchers are taking advantage of the selective permeability of BBB transport facilitating peptides or sugars and other penetrating molecules to deliver therapeutic agents to the brain[265,266] For example, it has been shown that when the IONPs are coated with a co-polymer of chitosan (a polysaccharide natural polymer) and PEG (d_H = 30 nm), they can pass the BBB.[86] This was attributed to (1) the high lipid solubility of the amphiphilic PEG that

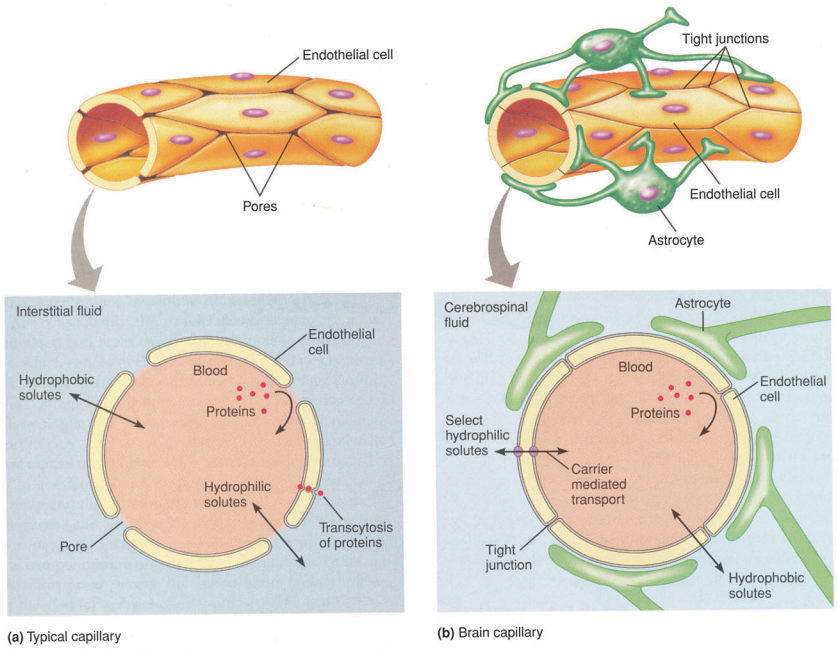

Fig. 10 Comparison of the typical blood capillaries found in most parts of the body (left) with the blood brain barrier (BBB, right). Small hydrophilic molecules can diffuse between blood and interstitial fluids through the pores between the endothelial cells in normal capillaries. Hydrophobic molecules and large size proteins can only pass this barrier by transcytosis. Endothelial cells in brain capillaries are connected by tight junctions. Proteins transcytosis is not possible in BBB and only selected hydrophilic molecules can pass the barrier by mediated carriers. Hydrophobic molecules can cross the BBB by transcytosis. Re-printed with permission from ref. 272. Copyright 2008, Pearson Education, Inc.

increases the endothelial permeability of the IONPs, (2) the electrostatic interaction between the cationic chitosan and negatively charged brain endothelium that may facilitate the adsorptive-mediated transport across the BBB and (3) the small hydrodynamic size of the IONPs.[86] As another example, intraperitoneal injection of silica coated magnetic nanoparticles has been reported as an effective method for facilitating the passage of the IONPs through the BBB.[256] This was described based on probable entry of the nanoparticles into the brain from discontinuities of the BBB in ganglia. Raut *et al.*[267] have shown that application of an external magnetic field can also enhance the permeability of the BBB; however, the mechanisms of overcoming this barrier through these approaches and possible adverse effects when nanoparticles pass BBB are still under investigation.[268] A recent study used stereotactic injection of the IONPs to brain for effective stimulation of the neurons at deep brain tissues using an external magnetic field.[269] This opens new possibilities for treatment of various brain diseases such as Alzheimer or Parkinson using IONPs. The nanoparticles were in the injected area one month after their administration. However, the long-term biodistribution and clearance mechanisms and kinetics of these nanoparticles require further investigations. Preliminary studies by Engberink *et al.*[270] suggest that cervical lymph nodes play a key role as a drainage pathway for the IONPs accumulated in the brain after passing the BBB. The exact clearance mechanisms of the IONPs from the brain and their probable side-effects (*e.g.* human neurodegenerative diseases due to changes in brain iron homeostasis) require extensive studies.[271]

Tumors. Fast growing tumors require new blood vessels (neovascularization) or rerouting of the existing vessels adjacent to the tumors to provide enough oxygen and nutrition for their survival.[273] This generates abnormal fenestrated endothelial structures around the tumors that are highly permeable for IONPs.[201,274] These leaky vessels, which lack any associated lymphatic drainage drive a unique process known as the enhanced permeability and retention (EPR) effect (Fig. 11) that is helpful in the effective delivery of the IONPs to the solid tumors.[275] These inter-endothelial pores can be as large as a few micrometers.[273,276] However, the desired nanoparticle hydrodynamic size range to evade MPS and renal elimination and enter the tumors by EPR is variably reported to be 30–200 nm by Albanese *et al.*,[10] 10–100 nm by Ranganathan *et al.*[277] and 50–600 nm (preferably smaller than 100 nm) by Melancon *et al.*[73] Further, the exact range of the pore sizes and effective NPs size can vary in different species and different types of tumors. Nanoparticles larger than 100 nm mainly get trapped in the extracellular spaces and cannot penetrate further after extravasation from these leaky blood vessels.[10,278] However, smaller IONPs (d_H < 20 nm) can penetrate deep into the perivascular area of the tumors, but they may have a short retention time because of hydraulic forces that can easily push them out of the tumor tissue.[10,73,279] After administration, these smaller nanoparticles can effectively evade liver and spleen uptake, but are rapidly eliminated from the blood by kidneys, specially for hydrodynamic sizes below 10–15 nm.[280] A recent study has shown that IONPs decorated with tumor-homing peptides that can specifically bind to fibrin and fibrin-associated

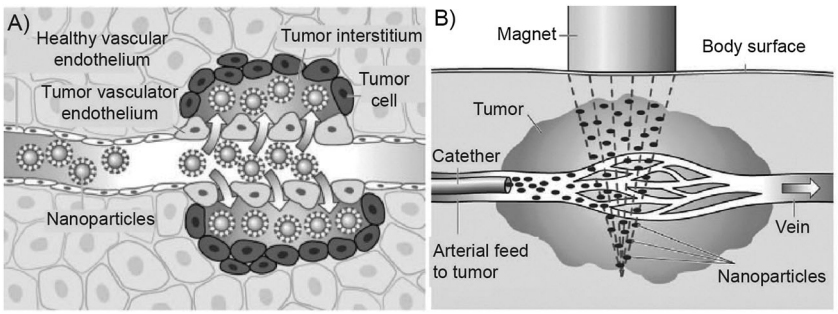

Fig. 11 (A) Tumors leaky vasculators and their enhanced permeability and retention (EPR). (B) Presence of an externally applied magnetic field can increase the accumulation of the IONPs in tumor area. Re-printed with permission from ref. 286. Copyright 2012, Elsevier B. V.

clotted plasma in tumor vessels can block blood flow through leaky tumor blood vessels and subsequently inhibit tumor growth.[281] Variations in the tumor targeted delivery of the IONPs through the EPR effect, might be due to differences in animal models and biological diversity of the tumors.[282]

In addition to the passive targeting mechanism described above, the IONPs can be directed to tumors, by attaching tumor specific antibodies or peptides to them.[283] These targeting molecules have high affinity for the unique receptor molecules found in specific tumor cells. Also, a magnetic field gradient can be used to drive the IONPs toward the desired location in the body.[30,284] A recent study, for example, shows that using an external magnet around the tumor sites, significantly enhances the targeting ability of the peptide loaded IONPs and decreases the liver uptake.[285] However, in some cases IONPs redistribution through the MPS organs (mainly liver and spleen) has been reported after removing the external magnetic field.[286] Such directed accumulation of the IONPs in the tumors is called active targeting.[73] The effect of active targeting on enhancing the accumulation of the IONPs in the tumor tissue is currently unclear, because of contradictory findings reported in the literature.[10] For effective targeting the nanoparticles loaded with antibodies or targeting peptides should have a long blood circulation time, which requires evading the elimination through MPS organs and kidneys. Therefore, as discussed in Section 2.1.4, the hydrodynamic size range of 10 nm $< d_H <$ 100 nm is required to minimize the MPS and renal clearance. Usually the hydrodynamic size increases considerably after conjugation of the targeting molecules to nanoparticles. This decreases the targeting ability due to shorter blood half-life. On the other hand, larger number of the targeting molecules can improve the targeting efficiency of the nanoparticles. Therefore, optimum numbers of targeting molecules should be added to IONPs in order to ensure the longest blood half-life.[287,288] The required number of targeting molecules on NPs depends on the type of the tumors and the affinity of these molecules for specific and selective binding to tumor cells.

Skin. For all the administration methods and routes (*e.g.* IV, oral, intrapulmonary and intratracheal delivery) described in this review, there is usually no distribution of the IONPs to the skin. Recent studies, however, showed a transdermal pathway and distribution of the IONPs directed through an incision in the skin. Lee *et al.*[289] studied the penetration of the IONPs into the skin when physical (sonophoresis) and chemical (oleic acid) stimuli were used to enhance the permeability of the stratum corneum (SC) by disrupting its lipid bilayer structure. It was shown that even in the presence of these enhancers, only restricted penetration of the IONPs to SC–stratum granulosum (SG) interface or upper SG layer was observed. Baroli *et al.*,[290] however, showed earlier that metallic nanoparticles can penetrate hair follicles and the SC layer and reach the skin epidermis, without application of any enhancer.

Ziv-Polat *et al.*[291] studied the clearance kinetics of the IONPs (d_C = 20 nm) from the incised rat skin. They found that 3 days after administration of the IONPs, they mostly resided in the extracellular spaces within the fibrin clot. The macrophages and fibroblasts actively took up the IONPs, so that after 8–14 days, IONPs were observed in both extracellular and intracellular spaces of these cells. Later, after 28 days, the majority of IONPs were cleared from the skin tissue with only negligible traces in intracellular vesicles of these cells. No further analyses were used to track the cleared IONPs or their degradation by-products in liver, spleen or kidneys.

3. Biodegradation and the fate of the IONPs in the body

3.1 Metabolic pathway of the IONPs

In a normal human body, 65% of the iron is present within the hemoglobin protein, 4% in myoglobin, 0.1% in transferrin and 15–30% in ferritin, which is mainly stored in the liver hepatocytes.[112] Ferritin ($d_H \sim 13$ nm) is composed of a protein shell surrounding an ultrasmall iron oxide nanoparticle in their central cavity ($d_C \sim 8$ nm) (Fig. 12).[123] It is believed that the mechanisms involved in intracellular degradation of any IONPs are very similar to those related to ferritin. In ferritin, the protein shell first gets dissolved by lysosomal proteases and then the internal iron oxide nanoparticles get released followed by rapid dissolution in acidic environment of the lysosomes.[123]

After degradation of the IONPs, there is an excess of iron in the organs, which needs to be regulated through the innate clearance mechanisms of the body.[292] Transferrin and ferritin are two principal iron–protein complexes that help to shuttle

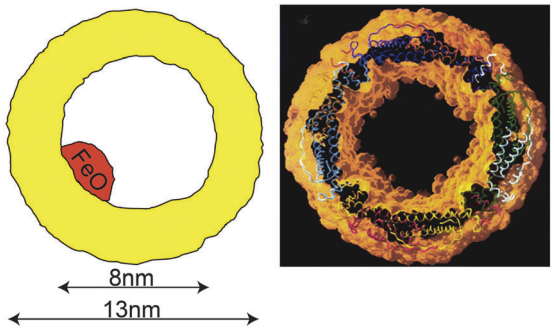

Fig. 12 Ferritin (~13 nm) is the main form of iron storage in the liver after degradation of IONPs in macrophages. It is formed from a protein shell (~13 nm) surrounding iron oxide ultrasmall nanoparticles in their central cavity (~8 nm). Re-printed with permission from ref. 123. Copyright 2010, Elsevier B. V.

and store the iron ions resulting from the degradation of the IONPs in the body.[62] Nissim[293] and Richter[294] were the pioneering researchers who reported the *in vivo* biodegradation of the iron oxide particles and role of transferrin and ferritin in the biodistribution of their degradation by-products more than six decades ago. Related investigations are still ongoing with the development of more advanced types of IONPs and characterization methods; for example, Levy *et al.*,[78] recently used a combination of multiple magnetic characterization techniques (EPR and SQUID) accompanied by intracellular TEM imaging and ICP quantification techniques (see Section 4 for description of these characterization methods) to precisely monitor the long-term (over three months) transformation of the iron oxide to ferritin in mouse liver and spleen.

Intravenously injected IONPs, taken up by the macrophages in different MPS organs, especially liver and spleen, get dissolved in the acidic environment of the lysosome compartments of these cells.[295,296] A slower IONPs degradation rate has been shown in spleen macrophages in comparison with liver Kupffer cells, as a result of the presence of less iron storage proteins available in spleen.[175] The degradation rate is also highly dependent on the type of materials coating the surface of the IONPs.[297] IONPs with coatings that allow limited water diffusion to their cores usually degrade slower in the macrophages.[298] Also, the degradation rate is slower for higher dosages of the injected IONPs.[299,300] The released iron ions bind to iron-binding apoferritin proteins existing in the cytoplasm of the macrophages and form ferritin.[118] Iron ions can easily detach from the ferritin and bind to apotransferrin to form transferrin.[301] Plasma transferrin circulates in the body to transport iron to different tissues such as bone marrow and muscles. In bone marrow they transform into hemoglobin in red blood cells (RBC) and in muscles they become myoglobin, an iron and oxygen binding protein responsible for carrying oxygen to muscle tissues in vertebrates.

In the bone marrow, transferrin can strongly bind to the receptors on the membrane of the erythroblasts, followed by endocytosis and release of the iron ions into the mitochondria to form hemoglobin, which later gets stored in the red blood cells as the principal oxygen carrier.[112,118] Senescent RBCs (the lifespan of RBCs is about 120 days in humans) are fragile and burst in the tight capillary spaces of the red pulp in the spleen, thus releasing their hemoglobin. This can cause an increase in the amount of iron in the spleen as reported by Levy *et al.*[78] MPS macrophages then phagocytize these hemoglobin molecules and transform a part of them into ferritin and then transferrin, which can again go back to bone marrow, be used to make new RBCs or get stored in the liver hepatocytes in the form of ferritin.[302] This ongoing cycle maintains the iron ions in the body for a long time with a slow clearance rate (Fig. 12).[301,303] Macrophages also transform a fraction of these hemoglobin molecules to bilirubin (a normal breakdown product of heme catabolism), which then gets excreted in bile and urine. If the amount of iron in the body is more than the available amount of apoferritin, large microscopic insoluble aggregates known as hemosiderin, form in the liver cells.[304] The iron-releasing rate from hemosiderin is much slower than ferritin.[304]

The iron ions released from the IONPs administered orally into the GI tract usually get absorbed through the small intestine. The apotransferrin protein secreted by the liver flows to the small intestine through the bile and then binds to these iron ions to form transferrin.[112] Transferrin molecules bind to the receptors of the intestinal epithelial cells and get internalized by pinocytosis and finally reach the plasma.[112] Transferrin transfers the iron ions into liver hepatocytes, where they release their loosely bound iron ions into the cytoplasm of these cells. Iron ions immediately bind with apoferritin to form ferritin as the main iron storage supply of the body and again iron enters the same metabolic cycle as the IV injected IONPs (Fig. 13). Generally, the GI absorption mechanism is much slower and less efficient than iron absorbed followed by IV injection of the IONPs, which is an important factor to consider when the IONPs are administrated for increasing the iron supply in the body for patients with anemia.[305,306] However, delivery of iron orally is safer since overdosing *via* this route is difficult.

The clearance of the iron released from inhaled IONPs in the lung also follows the same mechanism by incorporation of ferritin and transferrin. Alveolar macrophages take up and degrade the IONPs and form intracellular ferritin. Released ferritin transforms to transferrin in the bronchial and epithelial lining fluids and eventually gets cleared quickly by lung mucociliary system.[237] Transferrin can be also transported to the MPS system for the long-term storage, as described above.

The degradability and clearance of the coating materials should also be considered as an additional criterion for evaluation of the biodistribution of the IONPs. Radiolabeling of the iron oxide core and coating molecules is a common method for tracking of their movements along different excretion routes[307–309] or monitoring their integrity in blood circulation after administration.[310,311] For example, labeling of the iron oxide core by ^{56}Fe and dextran coating by ^{14}C tags, showed that dextran molecules have a much faster clearance kinetics compared to the iron core.[312] In a rat model, ~88.6% and ~12.9% of the injected coating molecules got degraded and cleared through urine and feces, respectively, after 56 days. On the other hand, only 16.8–21.8% and 1% of the administered iron was excreted in the feces and urine, respectively,

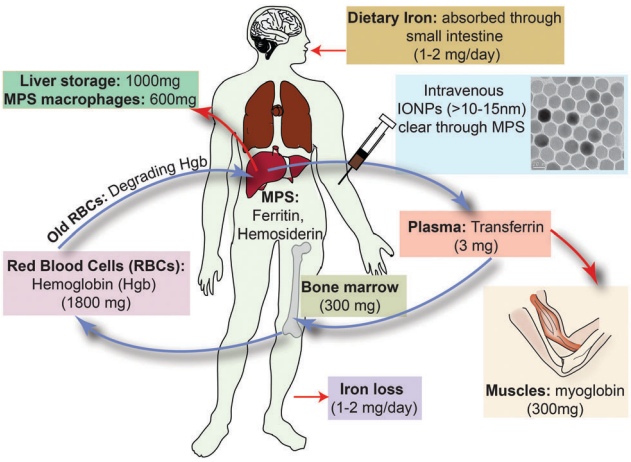

Fig. 13 IONPs biodegradation and general iron transport and metabolism pathway in the body. The intravenously injected IONPs, with hydrodynamic sizes larger than 10–15 nm, get degraded in MPS (or RES) macrophages and free iron ions transform to ferritin and hemosiderin iron–protein complexes. Ferritin can transform to transferrin and then get transported to bone marrow, where they are used for making hemoglobin in red blood cells (RBC) that circulate in the body. A part of this iron also forms myoglobin, an iron–protein complex carrying oxygen to muscles. Senescent RBCs are fragile and burst in the tight capillary spaces of the red pulp in the spleen and release their hemoglobin. This can cause an increase in the amount of iron in the spleen. MPS macrophages then phagocytize these hemoglobin molecules, form ferritin and again transform them into transferrin, which can go back to bone marrow to make new RBCs or get stored in the liver hepatocytes in the form of ferritin.

and the remaining dosage was still circulating in the body as part of the iron metabolic cycle even 84 days after injection. Alternatively, conjugation of fluorophores to the coating molecules and optical microscopy of the urine and feces have also been used to monitor clearance through the kidneys and the hepato-billiary pathways.[124] However, it is important to test the co-localization of the iron and fluorescent signals to make sure that the fluorescent signal is not just from the detached coating or fluorescent molecules due to their faster degradation and clearance rates. In a separate study, Tate *et al.*[313] determined the amount of the IONPs in mice organs, 14 and 580 days after injection, and showed the complete clearance of the IONPs after 580 days. Note that this report only showed the results 14 and 580 days after injection without any intermediate time points and therefore the exact clearance time cannot be exactly established.

Iron ions resulting from the degradation of the IONPs can be incorporated in the RBC hemoglobin either as ferrous (Fe^{2+}) or ferric (Fe^{3+}) ions. However, only Fe^{2+} ions are active in transporting the oxygen molecules between lung and other tissues.[314] Simply put, this is because ferric ions are at their highest state of oxidation and cannot react with the oxygen molecules.[315] Ferrous ions from hemoglobin, on the other hand, make weak and reversible bond with oxygen molecules, which are then released from red blood cells as they circulate.[112] Methemoglobin reductase enzyme can reactivate the non-functional ferric ions of the hemoglobin by reducing their oxidation state to ferrous.[315] Therefore, there might be some additional variations in the metabolic pathway of the different forms of IONPs (*i.e.* FeO, Fe_2O_3 or Fe_3O_4) and future studies can be helpful to investigate their pharmacokinetics more precisely.[316] Note that hemoglobin also transports carbon dioxide (CO_2), by forming a carbamate group between its terminal amino groups and CO_2 molecules.[317]

3.2 Organs half-lives

For safer application of the IONPs, the degradation rate of the IONPs in MPS organs should be specified by their half-life in each organ.[60] For example, it has been shown that for lower injected dosages (1 mg kg^{-1} body weight), IONP degradation in rat liver follows a mono-exponential decreasing rate, but for higher dosages (2 and 5 mg kg^{-1} body weight), it is a bi-exponential function comprising two separate fast and slow decay curves.[303] Knowing the tissue half-life is also important in monitoring the retention time of the IONPs in tumors when their therapeutic applications such as controlled release of the drugs are desired.[66,73,318] The half-lives of the IONPs in different organs can be determined using the same techniques that are used for measuring their blood half-lives.[319]

4. Methods for determining pharamacokinetics and biodistribution of IONPS

Various methods have been used for the detection of very low concentration of IONPs in blood and organs (*i.e.* nanomoles of iron per gram of the tissue).[320] These methods can be roughly categorized into imaging, spectroscopy and magnetometry. Imaging methods used for characterizing biodistribution of IONPs include, but are not limited to, transmission electron microscopy (TEM), optical microscopy, magnetic resonance imaging (MRI) and magnetic particle imaging (MPI) – a novel imaging modality that is sensitive solely to the magnetic signal from IONPs. The high magnification and resolution capabilities of TEM are helpful for observing IONPs distributed in the intracellular and extracellular regions of ultrathin tissue slices (*i.e.* 0.2 μm).[321] Furthermore, TEM offers additional tools such as electron beam diffraction[299] and elemental analysis[322,323] that can be used to differentiate iron oxides encapsulated in ferritin from the crystalline and superparamagnetic IONPs encapsulated in the lysosomes of liver and spleen macrophages; thus, TEM can provide detailed information about the pharmacokinetic and degradation pathways of IONPs.[78] It should be noted, however, that TEM needs electron transparent samples requiring costly and elaborate preparation procedures. Furthermore, due to its small field of view, TEM only provides limited information from selected regions of the sample. New emerging techniques can be used as more feasible alternatives for TEM. For example, in a recent study by Abe *et al.*,[130] a new non-destructive method called X-ray scanning analytical microscopy (XSAM) has been introduced for elemental mapping of iron in whole mice based on the analysis of energy-dispersed fluorescent X-rays in air, even when the samples contain water.

Histology, which is the analysis of tissue sections using optical microscopes, is a routine method that is usually more

cost-effective than TEM and can provide helpful information about the distribution of iron ions (from the blood or IONPs) in larger areas of tissue. Tissue sections are chemically stained with Prussian Blue or similar chemical agents that are specific for identifying iron ions. However, Prussian Blue staining for histology has its limitations – the technique is only usable for visualization of the iron ions and may not detect IONPs prior to degradation.[79] Also, it can't distinguish the endogenous iron in tissues from the administered iron. For quantitative studies, tissue sections (*e.g.* 100–200 mg) should be first dissolved in an acidic solution (*e.g.* 1 mL, aqua regia). Then Prussian Blue should be added to this solution, followed by absorbance measurements at 690 nm to quantify the amount of iron in each sample compared to tissues excised from control mice.[324] As an alternative method, IONPs intrinsic peroxidase-mimicking activity can be used to catalyze the oxidation of peroxidase substrates and produce a color foci at the site of the nanoparticles accumulation in tissues. Zhuang *et al.*[325] reported a higher sensitivity and therefore more accurate quantification of iron in tissues by using this method compared with traditional Prussian Blue staining.

In addition to *ex vivo* imaging methods described above, *in vivo* imaging with MRI and MPI can be used for characterizing biodistribution of IONPs. MRI is a non-destructive method that has been extensively used for biodistribution studies of IONPs in live animals.[326] Although MRI with T_2 contrast has been extensively used for *in vivo* tracking of the IONPs, it is not optimal when high concentrations of IONPs are localized in the organs (specially liver and spleen), which saturates the T_2 signal and results in dark images without any specifically useful information. Hoopes *et al.*[327] used a new technique named as ultra-short T_2 MRI to generate positive contrast from the IONPs and overcome the sensitivity limitations of the conventional MRI. MPI can also generate real-time positive contrast images that are solely generated from the IONPs. The technique is based on the nonlinear magnetic response of the IONPs to an applied AC magnetic field which induces a signal that is localized with a strong DC magnetic field gradient – additional details about the imaging technique can be found elsewhere.[328,329] This method is still under extensive investigations and will be commercially available in the near future.[330,331] Both MRI and MPI can detect very low iron concentrations down to nanograms per liter (ng L^{-1}) in solutions.[18,332]

Elemental analysis with spectroscopic methods, such as inductively coupled plasma-atomic emission spectroscopy (ICP-AES), is often used for quantitative chemical analysis. It is a destructive method that is used for quantifying the amount of elemental iron in the acid digested tissues.[201] Reports have shown that this technique can determine the iron concentrations down to orders of nanomoles of iron per gram of the tissue (nM Fe g^{-1} tissue)[320] However, like Prussian Blue staining, ICP-AES cannot differentiate the endogenous iron originating from the blood from the exogenous iron released from IONPs.[78,107,320] To resolve this challenge, Bellusci *et al.*[333] synthesized $MnFe_2O_4$ nanoparticles instead of pure magnetite (Fe_3O_4) and then using ICP, they measured the manganese concentration in organs to monitor the biodistribution of the injected nanoparticles more accurately. However, addition of manganese may raise some toxicity concerns or significantly change the magnetic performance of the IONPs.

Electron paramagnetic resonance (EPR), ferromagnetic resonance spectroscopy (FMR), magnetic susceptibility measurement (MSM) and superconducting quantum interference device (SQUID) are magnetometry techniques that can detect IONPs based on their magnetic properties and can be efficiently used to delineate iron from the IONPs and the endogenous iron in the blood pool. EPR has been recently used as a convenient method for quantification of the IONPs in tissues with very high sensitivity (*i.e.* nM Fe g^{-1} tissue).[285,320,324,334] Sample preparation is easy, but destructive and only usable for pieces of tissues excised from organs.[78,320,324] SQUID magnetometry is also a highly sensitive method that can detect even very weak magnetic fields in the body, such as mapping the brain or gastric activities (*i.e.* magnetoencephalography and magnetogastrography, respectively). For biodistribution studies, however, it has been used for quantifying IONPs from tissues excised and prepared similar to EPR method. Due to technical limitations and high costs of the device, it has been used only for limited number of IONPs biodistribution studies.[50,78,107]

Labeling of the IONPs by radioactive atoms (*e.g.* ^{59}Fe,[312,335] ^{111}In,[336] ^{51}Cr[337] or ^{69}Ge[309]) or near infrared fluorescent molecules (*e.g.* Cy5.5,[56,86,338] SBD/SDA[339] or VivoTag 800[275] fluorophores) have also been used for quantification of the IONPs in the tissues. These methods are based on loading of these radiating species onto IONPs and then measuring the emitted radioactive or fluorescent signals of the tissue samples or organs at different stages of the pharmacokinetic studies. Both techniques are relatively costly and require special training and facility, particularly for radioactive labeling. Also, loading of the fluorophores might change the hydrodynamic size of the IONPs. A non-radiation approach has been introduced for biodistribution studies of the IONPs. Crayton *et al.*[340] first doped different types of lanthanides (*i.e.* Ho, Eu, Gd and Sm) into different batches of IONPs with various sizes ($d_H \sim 15$, 29 and 70 nm) and surface charges (ranging from −20 to +14 mV). They injected these different types of IONPs to the same group of animals and then they used ICP to quantify each of these lanthanides in tissues to compare the pharmacokinetics and biodistribution pattern of these IONPs with different characteristics. Such studies help to determine the biodistribution of different types of the IONPs synergistically in only one experiment, without any concern for subject-to-subject variability. However, in a recent study, Naha *et al.*[341] doped bismuth into IONPs, since this element enhances the contrast in computed tomography (CT) imaging. They showed a significantly different clearance pharmacokinetics for iron and bismuth ions after degradation of the nanoparticles and therefore, such studies are only valid before the degradation of the IONPs starts. Also, similar to drugs and small molecules, theoretical modeling of the pharmacokinetics of the IONPs can be used as an efficient and cost-effective approach to predict the biodistribution of the IONPs.[342] However, these studies are still in their early stages.

5. *In vivo* toxicity of the IONPs

Iron oxide nanoparticles are generally considered as safe, biocompatible and non-toxic materials. LD-50 (the median lethal dose or the dose required to kill half of the tested animals during a specified time) of the uncoated iron oxide nanoparticles was reported to be 300–600 mg Fe kg^{-1} body weight.[343] This value was increased to 2000–6000 mg Fe kg^{-1} when the IONPs were coated with stabilizing and biocompatible dextran molecules.[343] A LD-50 value of 35 mmol Fe kg^{-1} was also reported for carboxy-dextran coated IONPs.[47] However, systematic toxicity studies are required when different types of molecules such as synthetic capping agents (*e.g.* oleic acid and oleyl amine) or different types of polymers, fluorophores and radioactive tags, or other therapeutic molecules are incorporated into the coating layer of the IONPs.[107]

5.1 Toxicity of the IONPs in animal models

In vivo toxicity studies of IONPs in animal models usually need long-term monitoring investigations for months or even years,[312,313] due to prolonged circulation of the degraded IONPs in the body. Measurement of the LD-50 of the materials historically raised some ethical concerns due to sacrificing of a large number of the animals.[344] However, use of traditional LD-50 testing is no longer required by the FDA. Different degradation rates and pharmacokinetics of the iron oxide cores and coating molecules make the studies even more complicated.[132] For example, while almost all the dextran molecules coating the IONPs were cleared from rats 56 days post-injection, about 80% of the injected IONPs were still circulating as iron–protein complexes in the blood after 84 days.[312] Due to this complexity, most of the toxicity results reported for IONPs are based on *in vitro* assays, in which the metabolic activity of a limited number of cell lines are measured for toxicity evaluation of IONPs. Although these experiments provide very helpful preliminary information, their results might not be necessarily applicable for all the different cell types and organs present in the body.[345] Nor may they satisfy regulatory requirements.

Toxicity in animal models is studied by evaluating changes in blood chemistries and variation of blood cell parameters, gene expression profiles in liver or change in gross or histologic features of organs as well as monitoring clinical and weight changes (among other endpoints) after administration of the IONPs.[107,132,346] Jain *et al.*[347] studied the toxicity of Pluronic coated IONPs (d_H = 186–206 nm in water) in rats, by monitoring the amount of alanine aminotransferase (ALT), aspartate aminotransferase (AST) and alkaline phosphatase (AKP) in serum after injection of the nanoparticles. Also, the amount of lipid hydroperoxide (LHPO) in different tissues were used to analyze the levels of their oxidative stresses due to administration of the IONPs. They showed that the IONPs only caused minor transient changes, over a period of 6–24 h in the liver enzyme levels. The small amount of oxidative stresses in different tissues also declined after 3 days. These results were also confirmed, by histological analyses of the organs, showing no apparent abnormal changes. In a recent study, Yang *et al.*,[132] analyzed the gene expression changes in mice liver after injection of IONPs with core sizes of 10, 20, 30 and 40 nm and hydrodynamic sizes of 14, 25, 34 and 43 nm, respectively. Their preliminary results (1 and 7 days after injection) showed that smaller nanoparticles (*i.e.* 10 and 20 nm IONPs) induced more changes in expression level of some susceptible genes such as Pcsk9 (proprotein convertase subtilisin/kexin type 9) and Hmox1 (heme oxygenase 1), indicating oxidative stress and possible changes in metabolic processes.

Gu *et al.*[107] also studied the *in vivo* toxicity of the monodisperse oleic acid capped IONPs (d_C = 5, 15 and 30 nm), coated with a layer of phospholipid–PEG co-polymer. Their hematology studies showed an increase in the number of neutrophils, 1 day after injection, which returned back to its normal amount through the next 30 days. This was attributed to the host defense response of the body to the presence of IONPs. There was also a consistent increase in ALT and AST enzymes possibly due to transfer of oleic acid molecules from liver macrophages to hepatocytes. All the other parameters were within the normal range. The differences between the results of this report and those shown by Jain *et al.*[347] for Pluronic coated IONPs was attributed to different species (mouse *vs.* rat) and the IONPs preparation approaches.

Monge-Fuentes *et al.*[346] also did a series of toxicity evaluations for dimercaptosuccinic acid (DMSA) coated IONPs in monkeys. Previous reports have shown some preferential accumulation in lung[348,349] and brain[350] for DMSA coated IONPs, due to some unknown mechanisms. However, no significant toxicity issue was observed in the nonhuman primate models during the 120-day study period.[346]

Feng *et al.*[351,352] reported that surface chemistry and size of the IONPs can affect the lipid, glucose and amino acid metabolism pathways, by disturbance of renal, hepatic and cardiac performance. Using high-resolution nuclear magnetic resonance (NMR) coupled with multivariate statistical analysis, they analyzed urine, plasma, spleen, liver and kidney in rats after administration of the dextran coated and uncoated IONPs. They observed metabolic changes such as elevation of urinary α-hydroxy-*n*-valerate, *o*- and *p*-HPA, and nicotinate, decreasing levels of urinary α-ketoglutarate, succinate and citrate, gradual increase in plasma glucose, saturated fatty acid, and individual amino acids and decrease of plasma unsaturated fatty acid and triacylglycerol.

Similar to IV injected IONPs, the type of the coating material plays an important role in toxicity level of the IONPs administrated through intranasal pathway. Park *et al.*[353] showed that intratracheal instillation of uncoated IONPs causes multiple adverse effects such as decreasing the level of intracellular reduced glutathione in the cells of bronchoalveolar lavage (BAL) fluid, increasing of pro-inflammatory cytokines in BAL fluid, expression of inflammation related genes and formation of microgranuloma. No toxicity was found when IONPs were coated by an anti-biofouling cross-linked polymer and administered through the same pathway.[236] However, silica coated IONPs did not show any pulmonary effect, but changed the level of the white blood cells in the blood and caused extramedullary hematopoiesis in the spleen.[244]

The oral administration of lower doses of the IONPs has also been reported as a generally safe route, with mild side effects such as nausea, vomiting or flatulence.[354] A study reported by Wang *et al.*[355] showed that increasing the dose of the IONPs ($d_H \sim 44$ nm), from 300 to 1200 mg Fe kg^{-1} mice weight, did not change the splenocyte proliferation and release of cytokines but changed the proportions of the T-lymphocyte subsets in peripheral blood, showing that higher doses influenced the immune function of the mice. Also, acute oral exposure to IONPs can cause severe side effects such as inhibition of acetylcholinestrase in red blood cells, inhibition of $Na^{(+)}$–$K^{(+)}$, $Mg^{(2+)}$, and $Ca^{(2+)}$-ATPases activities in brain and activation of the hepatotoxicity marker enzymes in serum and liver.[356] Di Bona *et al.*[357] also reported that intra-peritoneally injected IONPs can easily cross the placental barrier in pregnant mice and increase the risk of fetal deaths due to excessive accumulation of the IONPs in the fetal liver.

5.2 Clinical safety of the IONPs for human

Extensive pre-clinical and clinical research has been done during the last two decades to evaluate the side effects of IONPs administered to humans. However, these studies have been limited to dextran coated IONPs (*e.g.* Ferumoxide or Feridex, Fermoxytol or Feraheme, Resovist) by IV injection and silica coated IONPs (Ferumoxsil) by oral administration. Satisfactory toxicological profiles with no clinically significant side effects have been reported for these IONPs according to the standard pharmacological tests, following either IV injection[358] or oral administration.[354] A recent study using Ferucarbotran (Resovist) to map lymph node metastasis in 22 patients with thoracic squamous cell esophageal cancer showed no side effects from the IONPs.[359] Howarth *et al.*[360] used another type of dextran coated IONPs (Sinerem) for diagnosis of carotid inflammatory plaques in 20 patients without any adverse side effect. In another human trial, the safety of Ferumoxtran-10 was tested in 1777 adults and at least one adverse effect (*e.g.* back pain, pruritus, headache, and urticarial) was reported for 23.7% of the patients.[361] 7 patients (0.42%) experienced severe adverse effects (*e.g.* anaphylactic shock, chest pain, dyspnea, skin rash, oxygen saturation decreased, and 2 cases of hypotension). Also, one death was reported due to bolus injection of un-diluted IONPs. Bolus IV administration is no longer recommended for IONPs. This resulted in development of a safer formulation using lower molecular weight dextran to coat IONPs (Ferumoxytol or Feraheme).[358]

One of the most recent developments in the clinical applications of IONPs, is the approval of Ferumoxytol (or Feraheme) in June 2009 by the US Food and Drug Administration (FDA) for the treatment of iron deficiency in adults with chronic kidney disease.[8] Later in 2012, these IONPs also received European authorization, with a brand name of Rienso.[362] A high dose tolerability of up to 510 mg in one injection and an increase in hemoglobin level has been reported in patients using this product.[363] In a recent study, no serious adverse events were observed in 396 US patients following a total of 570 IV injections of these IONPs.[17] 22 patients reported minor adverse side effects such as headache, myalgia, nausea, chest discomfort, flushing, nasal congestion and pruritus or needed modified injections. Also, Hasan *et al.*[364] studied the unstable cerebral aneurysm by early uptake of these IONPs and none of the 22 patients experienced any adverse events. In a one-year retrospective observational study of 8666 US patients treated with IONPs, some severe adverse effects, including hypotension (0.12%), hypersensitivity (0.06%), dyspnoea (0.05%), loss of consciousness (0.03%), syncope (0.02%), unresponsive to stimuli (0.02%) and anaphylactoid reaction (0.02%) were reported.[358,365] Gastrointestinal effects such as nausea, vomiting, abdominal pain, diarrhea and constipation were among the most frequent adverse effects reported in a clinical study of 1562 patients reported from Europe and ~7.9% of the patients experienced some adverse effect.[362] However, some investigators still believe that the possible long-term safety effects of these IONPs have not been fully evaluated.[366]

6. Conclusions and future outlooks

Iron oxide nanoparticles incorporate excellent biocompatibility and safety factors with their unique magnetic properties, which can be easily optimized by tuning their size and distribution. Therefore, they are one of the most reliable candidates to be used in a wide range of biomedical applications such as cancer imaging and therapy, magnetic separation of malignant cells and stem cells labeling. Clinical success of the IONPs depends on three major parameters: pharmacokinetics, short and long-term tolerability in the body and therapeutic or diagnostic functionality in the desired organ. Biodistribution and toxicity of injected dextran coated iron oxide was first tested in animal models in the 1940's by Nissim.[293,367] In spite of the extensive research accompanied by development of more advanced characterization techniques and instruments during the previous six decades, there are still major un-answered questions regarding the preparation of safe and effective IONPs for different types of clinical diagnostic and therapeutic applications.

Different types of IONPs prepared by various synthesis methods and functionalized with a diverse range of coating molecules have been introduced during the last decades. However, clinical trials have been done for only two families of IONPs, *i.e.* those coated with polysaccharides or silica. In reality, various IONPs characteristics such as core and hydrodynamic size, morphology, size polydispersity, surface charge and type of the coating molecules affect the *in vivo* performance of the IONPs significantly. Other experimental variations such as method of administration, variations between animal models and humans, and different characterization techniques used can be also considered as influential factors. Preparation of standard databases for categorizing different pharmacokinetics, biodistribution and toxicity results based on specific IONPs characteristics and well-defined experimental factors can help investigators to find the required information in a much faster and cost effective way. The same approach has been successfully used for categorizing the mechanical, physical and chemical properties of a wide range of metallic alloys and compounds based on their elemental composition and complex processing parameters. These materials databases have been used as one of

the key tools during the industrial revolution of 20th century. This can help to efficiently address various clinical challenges by providing a wide range of valuable proof-of-concept results.

The effects of various additional molecular parameters such as mechanical flexibility or rigidity, molecular weight, density on the surface of the nanoparticles and molecular structure (*e.g.* presence of side-chains, functional groups on the backbone) of the coating molecules on pharmacokinetic performance and consistency of the IONPs need to be studied systematically. Also, effects of size, administered dose and crystalline structure of the iron oxide (amorphous, FeO, Fe_2O_3 or Fe_3O_4) on their degradation rates in MPS macrophages and transformation to plasma ferritin are still unknown. Recently developed characterization tools with higher mass sensitivities should be utilized to study these effects in more accurate ways.

Acknowledgements

This work was supported by NIH grants 1RO1EB013689-01 (National Institute of Biomedical Imaging and Bioengineering, NIBIB), 2R42EB013520-02A1 and 1R41EB013520-01.

References

1 K. M. Krishnan, *IEEE Trans. Magn.*, 2010, **46**, 2523–2558.
2 J. E. Rosen, L. Chan, D. B. Shieh and F. X. Gu, *Nanomedicine-Nanotechnology Biology and Medicine*, 2012, **8**, 275–290.
3 M. A. McAteer, A. M. Akhtar, C. von zur Muhlen and R. P. Choudhury, *Atherosclerosis*, 2010, **209**, 18–27.
4 H. Arami, Z. Stephen, O. Veiseh and M. Zhang, *Adv. Polym. Sci.*, 2011, **243**, 163–184.
5 F. M. Kievit, O. Veiseh, N. Bhattarai, C. Fang, J. W. Gunn, D. Lee, R. G. Ellenbogen, J. M. Olson and M. Q. Zhang, *Adv. Funct. Mater.*, 2009, **19**, 2244–2251.
6 S. M. C. Berman, P. Walczak and J. W. M. Bulte, *Wiley Interdiscip. Rev.: Nanomed. Nanobiotechnol.*, 2011, **3**, 343–355.
7 H. Y. Xu, Z. P. Aguilar, L. Yang, M. Kuang, H. W. Duan, Y. H. Xiong, H. Wei and A. Wang, *Biomaterials*, 2011, **32**, 9758–9765.
8 M. Lu, M. H. Cohen, D. Rieves and R. Pazdur, *Am. J. Hematol.*, 2010, **85**, 315–319.
9 N. Khlebtsov and L. Dykman, *Chem. Soc. Rev.*, 2011, **40**, 1647–1671.
10 A. Albanese, P. S. Tang and W. C. W. Chan, *Annu. Rev. Biomed. Eng.*, 2012, **14**, 1–16.
11 O. Veiseh, J. W. Gunn and M. Zhang, *Adv. Drug Delivery Rev.*, 2010, **62**, 284–304.
12 K. E. Sapsford, W. R. Algar, L. Berti, K. B. Gemmill, B. J. Casey, E. Oh, M. H. Stewart and I. L. Medintz, *Chem. Rev.*, 2013, **113**, 1904–2074.
13 F. M. Kievit and M. Q. Zhang, *Acc. Chem. Res.*, 2011, **44**, 853–862.
14 S. Laurent, J. L. Bridot, L. V. Elst and R. N. Muller, *Future Med. Chem.*, 2010, **2**, 427–449.
15 C. Tassa, S. Y. Shaw and R. Weissleder, *Acc. Chem. Res.*, 2011, **44**, 842–852.
16 A. J. Cole, A. E. David, J. X. Wang, C. J. Galban, H. L. Hill and V. C. Yang, *Biomaterials*, 2011, **32**, 2183–2193.
17 M. Auerbach, J. A. Pappadakis, H. Bahrain, S. A. Auerbach, H. Ballard and N. V. Dahl, *Am. J. Hematol.*, 2011, **86**, 860–862.
18 H. Arami, R. M. Ferguson, A. P. Khandhar and K. M. Krishnan, *Med. Phys.*, 2013, **40**, 071904.
19 B. H. Kim, N. Lee, H. Kim, K. An, Y. I. Park, Y. Choi, K. Shin, Y. Lee, S. G. Kwon, H. B. Na, J.-G. Park, T.-Y. Ahn, Y.-W. Kim, W. K. Moon, S. H. Choi and T. Hyeon, *J. Am. Chem. Soc.*, 2011, **133**, 12624–12631.
20 A. P. Khandhar, R. M. Ferguson, H. Arami and K. M. Krishnan, *Biomaterials*, 2013, **34**, 3837–3845.
21 M. Gould, R. J. Barbour, N. Thomas, H. Arami, K. M. Krishnan and K.-M. C. Fu, *Appl. Phys. Lett.*, 2014, **105**, 072406.
22 R. Weissleder, G. Elizondo, J. Wittenberg, C. A. Rabito, H. H. Bengele and L. Josephson, *Radiology*, 1990, **175**, 489–493.
23 C. Chambon, O. Clement, A. Leblanche, E. Schoumanclaeys and G. Frija, *Magn. Reson. Imaging*, 1993, **11**, 509–519.
24 E. X. Wu, H. Y. Tang and J. H. Jensen, *NMR Biomed.*, 2004, **17**, 478–483.
25 M. E. Kooi, V. C. Cappendijk, K. Cleutjens, A. G. H. Kessels, P. Kitslaar, M. Borgers, P. M. Frederik, M. Daemen and J. M. A. van Engelshoven, *Circulation*, 2003, **107**, 2453–2458.
26 M. Beaumont, B. Lemasson, R. Farion, C. Segebarth, C. Remy and E. L. Barbier, *J. Cereb. Blood Flow Metab.*, 2009, **29**, 1714–1726.
27 N. Beckmann, C. Cannet, A. L. Babin, F. X. Ble, S. Zurbruegg, R. Kneuer and V. Dousset, *Wiley Interdiscip. Rev.: Nanomed. Nanobiotechnol.*, 2009, **1**, 272–298.
28 R. Weissleder, A. Bogdanov, E. A. Neuwelt and M. Papisov, *Adv. Drug Delivery Rev.*, 1995, **16**, 321–334.
29 K. Lee, C. Cheong, K. S. Hong, E. K. Koh, M. Kim, H. S. Shin, Y. N. Kim and S. H. Lee, *J. Korean Phys. Soc.*, 2008, **53**, 2535–2539.
30 H. W. Yang, M. Y. Hua, H. L. Liu, C. Y. Huang, R. Y. Tsai, Y. J. Lu, J. Y. Chen, H. J. Tang, H. Y. Hsien, Y. S. Chang, T. C. Yen, P. Y. Chen and K. C. Wei, *Biomaterials*, 2011, **32**, 6523–6532.
31 M. Taupitz, S. Wagner, J. Schnorr, I. Kravec, H. Pilgrimm, H. Bergmann-Fritsch and B. Hamm, *Invest. Radiol.*, 2004, **39**, 394–405.
32 S. J. McLachlan, M. R. Morris, M. A. Lucas, R. A. Fisco, M. N. Eakins, D. R. Fowler, R. B. Scheetz and A. Y. Olukotun, *J. Magn. Reson. Imaging*, 1994, **4**, 301–307.
33 C. D. Constantinides, J. Rogers, D. A. Herzka, F. E. Boada, D. Bolar, D. Kraitchman, J. Gillen and P. A. Bottomley, *Magn. Reson. Med.*, 2001, **46**, 1164–1168.
34 F. Q. Zhao, M. Williams, X. Meng, D. C. Welsh, A. Coimbra, E. D. Crown, J. J. Cook, M. O. Urban, R. Hargreaves and D. S. Williams, *NeuroImage*, 2008, **40**, 133–147.
35 M. Sigovan, L. Boussel, A. Sulaiman, D. Sappey-Marinier, H. Alsaid, C. Desbleds-Mansard, D. Ibarrola, D. Gamondes, C. Corot, E. Lancelot, J. S. Raynaud, V. Vives, C. Lacledere,

X. Violas, P. C. Douek and E. Canet-Soulas, *Radiology*, 2009, **252**, 401–409.
36 M. Sigovan, A. Bessaad, H. Alsaid, E. Lancelot, C. Corot, B. Neyran, N. Provost, Z. Majd, M. Breisse and E. Canet-Soulas, *Invest. Radiol.*, 2010, **45**, 702–707.
37 R. Sigal, T. Vogl, J. Casselman, G. Moulin, F. Veillon, R. Hermans, F. Dubrulle, J. Viala, J. Bosq, M. Mack, M. Depondt, C. Mattelaer, P. Petit, P. Champsaur, S. Reihm, Y. Dadashitazehozi, T. de Jaegere, G. Marchal, D. Chevalier, L. Lemaitre, C. Kubiak, R. Helmberger and P. Halimi, *E. Radiol.*, 2002, **12**, 1104–1113.
38 H. H. Bengele, S. Palmacci, J. Rogers, C. W. Jung, J. Crenshaw and L. Josephson, *Magn. Reson. Imaging*, 1994, **12**, 433–442.
39 O. Clément, N. Siauve, C. A. Cuénod and G. Frija, *Magn. Reson. Imaging*, 1998, **9**, 167–182.
40 K. C. Briley-Saebo, V. Mani, F. Hyafil, J.-C. Cornily and Z. A. Fayad, *Magn. Reson. Med.*, 2008, **59**, 721–730.
41 D. Simberg, J. H. Park, P. P. Karmali, W. M. Zhang, S. Merkulov, K. McCrae, S. N. Bhatia, M. Sailor and E. Ruoslahti, *Biomaterials*, 2009, **30**, 3926–3933.
42 C. Chapon, F. Franconi, L. Lemaire, L. Marescaux, P. Legras, J. P. Saint-Andre, B. Denizot and J. J. Le Jeune, *Invest. Radiol.*, 2003, **38**, 141–146.
43 V. Rousseau, D. Pouliquen, F. Darcel, P. Jallet and J. J. Le Jeune, *Magn. Reson. Mater. Phys., Biol. Med.*, 1998, **6**, 13–21.
44 B. B. Frericks, F. Wacker, C. Loddenkemper, S. Valdeig, B. Hotz, K. J. Wolf, B. Misselwitz, A. Kuhl and J. C. Hoffmann, *Invest. Radiol.*, 2009, **44**, 23–30.
45 G. H. Simon, J. von Vopelius-Feldt, Y. J. Fu, J. Schlegel, G. Pinotek, M. F. Wendland, M. H. Chen and H. E. Daldrup-Link, *Invest. Radiol.*, 2006, **41**, 45–51.
46 K. Lind, M. Kresse, N. P. Debus and R. H. Muller, *J. Drug Targeting*, 2002, **10**, 221–230.
47 S. A. Schmitz, S. E. Coupland, R. Gust, S. Winterhalter, S. Wagner, M. Kresse, W. Semmler and K. J. Wolf, *Invest. Radiol.*, 2000, **35**, 460–471.
48 W. Li, S. Tutton, A. T. Vu, L. Pierchala, B. S. Y. Li, J. M. Lewis, P. V. Prasad and R. R. Edelman, *J. Magn. Reson. Imaging*, 2005, **21**, 46–52.
49 B. Tomanek, U. Iqbal, B. Blasiak, A. Abulrob, H. Albaghdadi, J. R. Matyas, D. Ponjevic and G. R. Sutherland, *Neuro-Oncology*, 2012, **14**, 53–63.
50 J.-H. Park, G. von Maltzahn, L. Zhang, A. M. Derfus, D. Simberg, T. J. Harris, E. Ruoslahti, S. N. Bhatia and M. J. Sailor, *Small*, 2009, **5**, 694–700.
51 J. Hamzah, V. R. Kotamraju, J. W. Seo, L. Agemy, V. Fogal, L. M. Mahakian, D. Peters, L. Roth, M. K. J. Gagnon, K. W. Ferrara and E. Ruoslahti, *Proc. Natl. Acad. Sci. U. S. A.*, 2011, **108**, 7154–7159.
52 G. Wang, S. Inturi, N. J. Serkova, S. Merkulov, K. McCrae, S. E. Russek, N. K. Banda and D. Simberg, *ACS Nano*, 2014, **8**, 12437–12449.
53 C. Nolte-Ernsting, G. Adam, A. Bucker, S. Berges, A. Bjornerud and R. W. Gunther, *Am. J. Roentgenol.*, 1998, **171**, 107–113.
54 R. Bachmann, R. Conrad, B. Kreft, O. Luzar, W. Block, S. Flacke, D. Pauleit, F. Traber, J. Gieseke, K. Saebo and H. Schild, *J. Magn. Reson. Imaging*, 2002, **16**, 190–195.
55 D. Weishaupt, P. R. Hilfiker, M. Schmidt and J. F. Debatin, *Cardiovascular and Interventional Radiology*, 1999, **22**, 321–325.
56 M. J.-E. Lee, O. Veiseh, N. Bhattarai, C. Sun, S. J. Hansen, S. Ditzler, S. Knoblaugh, D. Lee, R. Ellenbogen, M. Zhang and J. M. Olson, *PLoS One*, 2010, **5**, e9536.
57 K. L. Hultman, A. J. Raffo, A. L. Grzenda, P. E. Harris, T. R. Brown and S. O'Brien, *ACS Nano*, 2008, **2**, 477–484.
58 K. C. Briley-Saebo, Y. S. Cho, P. X. Shaw, S. K. Ryu, V. Mani, S. Dickson, E. Izadmehr, S. Green, Z. A. Fayad and S. Tsimikas, *J. Am. Coll. Cardiol.*, 2011, **57**, 337–347.
59 S. Wagner, J. Schnorr, H. Pilgrimm, B. Hamm and M. Taupitz, *Invest. Radiol.*, 2002, **37**, 167–177.
60 J. Schnorr, M. Taupitz, S. Wagner, H. Pilgrimm, J. Hansel and B. Hamm, *J. Magn. Reson. Imaging*, 2000, **12**, 740–744.
61 P. Y. Brillet, F. Gazeau, A. Luciani, B. Bessoud, C. A. Cuenod, N. Siauve, J. N. Pons, J. Poupon and O. Clement, *European Radiology*, 2005, **15**, 1369–1377.
62 A. Ruiz, Y. Hernandez, C. Cabal, E. Gonzalez, S. Veintemillas-Verdaguer, E. Martinez and M. P. Morales, *Nanoscale*, 2013, **5**, 11400–11408.
63 A. P. Khandhar, R. M. Ferguson, H. Arami, S. J. Kemp and K. M. Krishnan, *IEEE Trans. Magn.*, 2015, **51**, 1–4.
64 A. P. Khandhar, S. J. Kemp, R. M. Ferguson and K. M. Krishnan, in *5th International Workshop on Magnetic Particle Imaging (IWMPI)*, IEEE, Turkey, Istanbul, 2015, p. 1.
65 H. Arami, A. P. Khandhar, A. Tomitaka, E. Yu, P. W. Goodwill, S. M. Conolly and K. M. Krishnan, *Biomaterials*, 2015, **52**, 251–261.
66 B. Moffat, G. R. Reddy, P. McConville, D. E. Hall, T. L. Chenevert, R. R. Kopelman, R. Weissleder, A. Rehemtulla and B. D. Ross, *Mol. Imaging*, 2003, **2**, 324–332.
67 Y. Yang, Y. Yang, N. Yanasak, A. Schumacher and T. C. C. Hu, *Magn. Reson. Med.*, 2010, **63**, 33–40.
68 Y. D. Yang, J. M. Liu, Y. H. Yang, S. H. Cho and T. C. C. Hu, *Magn. Reson. Med.*, 2011, **66**, 1353–1361.
69 H. Xu, L. Cheng, C. Wang, X. Ma, Y. Li and Z. Liu, *Biomaterials*, 2011, **32**, 9364–9373.
70 F. M. Kievit, Z. R. Stephen, O. Veiseh, H. Arami, T. Z. Wang, V. P. Lai, J. O. Park, R. G. Ellenbogen, M. L. Disis and M. Q. Zhang, *ACS Nano*, 2012, **6**, 2591–2601.
71 M. Ferrari, *Nat. Rev. Cancer*, 2005, **5**, 161–171.
72 D. Peer, J. M. Karp, S. Hong, O. C. FaroKhzad, R. Margalit and R. Langer, *Nat. Nanotechnol.*, 2007, **2**, 751–760.
73 M. P. Melancon, W. Lu and C. Li, *MRS Bull.*, 2009, **34**, 415–421.
74 I. Singh, *Textbook of Human Histology*, Jaypee Brothers Publishers, New Delhi, India, 2006.
75 P. J. Murray and T. A. Wynn, *Nat. Rev. Immunol.*, 2011, **11**, 723–737.
76 K. Saijo and C. K. Glass, *Nat. Rev. Immunol.*, 2011, **11**, 775–787.
77 C. Shi and E. G. Pamer, *Nat. Rev. Immunol.*, 2011, **11**, 762–774.

78 M. Levy, N. Luciani, D. Alloyeau, D. Elgrabli, V. Deveaux, C. Pechoux, S. Chat, G. Wang, N. Vats, F. Gendron, C. Factor, S. Lotersztajn, A. Luciani, C. Wilhelm and F. Gazeau, *Biomaterials*, 2011, **32**, 3988–3999.
79 A. J. Cole, A. E. David, J. X. Wang, C. J. Galban and V. C. Yang, *Biomaterials*, 2011, **32**, 6291–6301.
80 A. Beduneau, Z. Ma, C. B. Grotepas, A. Kabanov, B. E. Rabinow, N. Gong, R. L. Mosley, H. Dou, M. D. Boska and H. E. Gendelman, *PLoS One*, 2009, **4**, e4343.
81 S. W. Jones, R. A. Roberts, G. R. Robbins, J. L. Perry, M. P. Kai, K. Chen, T. Bo, M. E. Napier, J. P. Y. Ting, J. M. DeSimone and J. E. Bear, *J. Clin. Invest.*, 2013, **123**, 3061–3073.
82 B. R. Smith, E. E. B. Ghosn, H. Rallapalli, J. A. Prescher, T. Larson, L. A. Herzenberg and S. S. Gambhir, *Nat. Nanotechnol.*, 2014, **9**, 481–487.
83 D. Simberg, T. Duza, J.-H. Park, M. Essler, J. Pilch, L. Zhang, A. M. Derfus, M. Yang, R. M. Hoffman, S. Bhatia, M. J. Sailor and E. Ruoslahti, *Proc. Natl. Acad. Sci. U. S. A.*, 2007, **104**, 932–936.
84 C. Wang, X. Q. Sun, L. Cheng, S. N. Yin, G. B. Yang, Y. G. Li and Z. Liu, *Adv. Mater.*, 2014, **26**, 4794–4802.
85 V. I. Shubayev, T. R. Pisanic II and S. Jin, *Adv. Drug Delivery Rev.*, 2009, **61**, 467–477.
86 O. Veiseh, C. Sun, C. Fang, N. Bhattarai, J. Gunn, F. Kievit, K. Du, B. Pullar, D. Lee, R. G. Ellenbogen, J. Olson and M. Zhang, *Cancer Res.*, 2009, **69**, 6200–6207.
87 R. A. M. Heesakkers, G. J. Jager, A. M. Hovels, B. de Hoop, H. C. M. van den Bosch, F. Raat, J. A. Witjes, P. F. A. Mulders, C. H. van der Kaa and J. O. Barentsz, *Radiology*, 2009, **251**, 408–414.
88 G. Nakai, M. Matsuki, T. Harada, N. Tanigawa, T. Yamada, J. Barentsz and Y. Narumi, *J. Magn. Reson. Imaging*, 2011, **34**, 557–562.
89 A. Yilmaz, S. Rosch, H. Yildiz, S. Klumpp and U. Sechtem, *Circulation*, 2012, **126**, 1932–1934.
90 D. Qiu, G. Zaharchuk, T. Christen, W. W. Ni and M. E. Moseley, *NeuroImage*, 2012, **62**, 1726–1731.
91 C. Kleinschnitz, T. Bendszus, M. Frank, T. Solymosi, K. V. Toyka and G. Stoll, *J. Cereb. Blood Flow Metab.*, 2003, **23**, 1356–1361.
92 M. S. A. Deloire, T. Touil, B. Brochet, V. Dousset, J. M. Caille and K. G. Petry, *Mult. Scler.*, 2004, **10**, 540–548.
93 S. Valable, E. L. Barbier, M. Bemaudin, S. Roussel, C. Segebarth, E. Petit and C. Remy, *NeuroImage*, 2008, **40**, 973–983.
94 E. Penno, C. Johnsson, L. Johansson and H. Ahlstrom, *Acta Radiol.*, 2006, **47**, 264–271.
95 A. Nchimi, O. Defawe, D. Brisbois, T. K. Y. Broussaud, J.-O. Defraigne, P. Magotteaux, B. Massart, J.-M. Serfaty, X. Houard, J.-B. Michel and N. Sakalihasan, *Radiology*, 2010, **254**, 973–981.
96 N. Beckmann, C. Cannet, S. Zurbruegg, R. Haberthur, J. Li, C. Pally and C. Bruns, *Radiology*, 2006, **240**, 717–724.
97 Y. Lee, J. W. Ryu, H. Chang, J. Y. Sohn, K. W. Lee, C. W. Woo, H. J. Kang, S. Y. Jeong, E. K. Choi and J. S. Lee, *Magn. Reson. Med.*, 2010, **64**, 72–79.
98 X. Chen, R. Wong, I. Khalidov, A. Y. Wang, J. Leelawattanachai, Y. Wang and M. M. Jin, *Biomaterials*, 2011, **32**, 7651–7661.
99 J. V. Jokerst, T. Lobovkina, R. N. Zare and S. S. Gambhir, *Nanomedicine*, 2011, **6**, 715–728.
100 F. Braet and E. Wisse, *Comp. Hepatol.*, 2002, **1**, 1.
101 H. Sarin, *J. Angiog. Res.*, 2010, **2**, 1–19.
102 M. Saito, T. Matsuura, K. Nagatsuma, K. Tanaka, H. Maehashi, K. Shimizu, Y. Hataba, F. Kato, I. Kashimori, H. Tajiri and F. Braet, *J. Membr. Biol.*, 2007, **217**, 115–121.
103 R. Gref, Y. Minamitake, M. T. Peracchia, V. Trubetskoy, V. Torchilin and R. Langer, *Science*, 1994, **263**, 1600–1603.
104 J. Huang, L. Bu, J. Xie, K. Chen, Z. Cheng, X. Li and X. Chen, *ACS Nano*, 2010, **4**, 7151–7160.
105 J. T. Ferrucci and D. D. Stark, *Am. J. Roentgenol.*, 1990, **155**, 943–950.
106 D. P. Cormode, G. O. Skajaa, A. Delshad, N. Parker, P. A. Jarzyna, C. Calcagno, M. W. Galper, T. Skajaa, K. C. Briley-Saebo, H. M. Bell, R. E. Gordon, Z. A. Fayad, S. L. C. Woo and W. J. M. Mulder, *Bioconjugate Chem.*, 2011, **22**, 353–361.
107 L. Gu, R. H. Fang, M. J. Sailor and J.-H. Park, *ACS Nano*, 2012, **6**, 4947–4954.
108 T. Seested, R. S. Appa, E. I. Christensen, Y. A. Ioannou, T. N. Krogh, D. M. Karpf and H. M. Nielsen, *Thromb. Res.*, 2011, **127**, 356–362.
109 S.-J. Cheong, C.-M. Lee, S.-L. Kim, H.-J. Jeong, E.-M. Kim, E.-H. Park, D. W. Kim, S. T. Lim and M.-H. Sohn, *Int. J. Pharm.*, 2009, **372**, 169–176.
110 C.-M. Lee, H.-J. Jeong, E.-M. Kim, D. W. Kim, S. T. Lim, H. T. Kim, I.-K. Park, Y. Y. Jeong, J. W. Kim and M.-H. Sohn, *Magn. Reson. Med.*, 2009, **62**, 1440–1446.
111 B. E. Van Beers, C. Sempoux, R. Materne, M. Delos and A. M. Smith, *J. Magn. Reson. Imaging*, 2001, **13**, 594–599.
112 A. C. Guyton and J. E. Hall, *Textbook of Medical Physiology*, Elsevier, PA, USA, 12th edn, 2011.
113 C.-C. Huang, C.-Y. Tsai, H.-S. Sheu, K.-Y. Chuang, C.-H. Su, U. S. Jeng, F.-Y. Cheng, C.-H. Su, H.-Y. Lei and C.-S. Yeh, *ACS Nano*, 2011, **5**, 3905–3916.
114 M. Demoy, J. P. Andreux, C. Weingarten, B. Gouritin, V. Guilloux and P. Couvreur, *Pharm. Res.*, 1999, **16**, 37–41.
115 S. Pillai and A. Cariappa, *Nat. Rev. Immunol.*, 2009, **9**, 767–777.
116 V.-Q. Hieu, M.-K. Yoo, H.-J. Jeong, H.-J. Lee, M. Muthiah, J. H. Rhee, J.-H. Lee, C.-S. Cho, Y. Y. Jeong and I.-K. Park, *Acta Biomater.*, 2011, **7**, 3935–3945.
117 M. G. Harisinghani, J. Barentsz, P. F. Hahn, W. M. Deserno, S. Tabatabaei, C. H. van de Kaa, J. de la Rosette and R. Weissleder, *N. Engl. J. Med.*, 2003, **348**, U2491–U2495.
118 C. Corot, P. Robert, J.-M. Idee and M. Port, *Adv. Drug Delivery Rev.*, 2006, **58**, 1471–1504.
119 F. Alexis, E. Pridgen, L. K. Molnar and O. C. Farokhzad, *Mol. Pharmaceutics*, 2008, **5**, 505–515.
120 J. P. M. Almeida, A. L. Chen, A. Foster and R. Drezek, *Nanomedicine*, 2011, **6**, 815–835.
121 S. C. Satchell and F. Braet, *American Journal of Physiology-Renal Physiology*, 2009, **296**, F947–F956.

122 A. B. Fogo and V. Kon, *Int. J. Biochem. Cell Biol.*, 2010, **42**, 1388–1397.
123 T. Skotland, T.-G. Iversen and K. Sandvig, *Nanomedicine-Nanotechnology Biology and Medicine*, 2010, **6**, 730–737.
124 G. Lamanna, M. Kueny-Stotz, H. Mamlouk-Chaouachi, C. Ghobril, B. Basly, A. Bertin, I. Miladi, C. Billotey, G. Pourroy, S. Begin-Colin and D. Felder-Flesch, *Biomaterials*, 2011, **32**, 8562–8573.
125 J. E. Zuckerman, C. H. J. Choi, H. Han and M. E. Davis, *Proc. Natl. Acad. Sci. U. S. A.*, 2012, **109**, 3137–3142.
126 C. Glaus, R. Rossin, M. J. Welch and G. Bao, *Bioconjugate Chem.*, 2010, **21**, 715–722.
127 K. Chen, J. Xie, H. Xu, D. Behera, M. H. Michalski, S. Biswal, A. Wang and X. Chen, *Biomaterials*, 2009, **30**, 6912–6919.
128 N. Arsalani, H. Fattahi, S. Laurent, C. Burtea, L. Vander Elst and R. N. Muller, *Contrast Media Mol. Imaging*, 2012, **7**, 185–194.
129 Y. F. Tan, P. Chandrasekharan, D. Maity, C. X. Yong, K.-H. Chuang, Y. Zhao, S. Wang, J. Ding and S.-S. Feng, *Biomaterials*, 2011, **32**, 2969–2978.
130 S. Abe, I. Kida, M. Esaki, T. Akasaka, M. Uo, T. Hosono, Y. Sato, B. Jeyadevan, Y. Kuboki, M. Morita, K. Tohji and F. Watari, *Bio-Med. Mater. Eng.*, 2009, **19**, 213–220.
131 L. Yang, H. Mao, Z. Cao, Y. A. Wang, X. Peng, X. Wang, H. K. Sajja, L. Wang, H. Duan, C. Ni, C. A. Staley, W. C. Wood, X. Gao and S. Nie, *Gastroenterology*, 2009, **136**, 1514–1525.
132 L. Yang, H. Kuang, W. Zhang, Z. P. Aguilar, Y. Xiong, W. Lai, H. Xu and H. Wei, *Nanoscale*, 2015, **7**, 625–636.
133 M. Varna, P. Ratajczak, I. Ferreira, C. Leboeuf, G. Bousquet and A. Janin, *J. Biomater. Nanobiotechnol.*, 2012, **3**, 269–279.
134 Z. Lin, N. A. Monteiro-Riviere and J. E. Riviere, *Wiley Interdiscip. Rev.: Nanomed. Nanobiotechnol.*, 2015, **7**, 189–217.
135 F. Roohi, J. Lohrke, A. Ide, G. Schuetz and K. Dassler, *Int. J. Nanomed.*, 2012, **7**, 4447–4458.
136 Y. X. J. Wang, S. M. Hussain and G. P. Krestin, *Eur. Radio.*, 2001, **11**, 2319–2331.
137 A. K. Gupta and S. Wells, *IEEE Transactions on Nanobioscience*, 2004, **3**, 66–73.
138 Y. Chen and B.-A. Chen, *Chin. J. Cancer*, 2010, **29**, 118–122.
139 A. Kunzmann, B. Andersson, T. Thurnherr, H. Krug, A. Scheynius and B. Fadeel, *Biochim. Biophys. Acta, Gen. Subj.*, 2011, **1810**, 361–373.
140 G. Fleige, F. Seeberger, D. Laux, M. Kresse, M. Taupitz, H. Pilgrimm and C. Zimmer, *Invest. Radiol.*, 2002, **37**, 482–488.
141 M. Longmire, P. L. Choyke and H. Kobayashi, *Nanomedicine*, 2008, **3**, 703–717.
142 S. H. Choi, W. K. Moon, J. H. Hong, K. R. Son, N. Cho, B. J. Kwon, J. J. Lee, J. K. Chung, H. S. Min and S. H. Park, *Radiology*, 2007, **242**, 137–143.
143 B. B. Pultrum, E. J. van der Jagt, H. L. van Westreenen, H. M. van Dullemen, P. Kappert, H. Groen, J. Sietsma, M. Oudkerk, J. T. M. Plukker and G. M. van Dam, *Cancer Imaging*, 2009, **9**, 19–28.
144 O. Veiseh, C. Sun, C. Fang, N. Bhattarai, J. Gunn, F. Kievit, K. Du, B. Pullar, D. Lee, R. G. Ellenbogen, J. Olson and M. Zhang, *Cancer Res.*, 2009, **69**, 6200–6207.
145 A. Iannone, R. L. Magin, T. Walczak, M. Federico, H. M. Swartz, A. Tomasi and V. Vannini, *Magn. Reson. Med.*, 1991, **22**, 435–442.
146 M. Di Marco, C. Sadun, M. Port, I. Guilbert, P. Couvreur and C. Dubernet, *Int. J. Nanomed.*, 2007, **2**, 609–622.
147 C. Fang, N. Bhattarai, C. Sun and M. Q. Zhang, *Small*, 2009, **5**, 1637–1641.
148 X.-H. Peng, X. Qian, H. Mao, A. Y. Wang, Z. Chen, S. Nie and D. M. Shin, *Int. J. Nanomed.*, 2008, **3**, 311–321.
149 H. Arami and K. M. Krishnan, *IEEE Trans. Magn.*, 2013, **49**, 3500–3503.
150 D. L. J. Thorek and A. Tsourkas, *Biomaterials*, 2008, **29**, 3583–3590.
151 C. Boyer, M. R. Whittaker, V. Bulmus, J. Q. Liu and T. P. Davis, *Nature Publishing Group Asia Materials*, 2010, **2**, 23–30.
152 S. Tong, S. Hou, Z. Zheng, J. Zhou and G. Bao, *Nano Lett.*, 2010, **10**, 4607–4613.
153 R. M. Ferguson, A. P. Khandhar, S. J. Kemp, H. Arami, E. U. Saritas, L. R. Croft, J. Konkle, P. W. Goodwill, A. Halkola, J. Rahmer, J. Borgert, S. M. Conolly and K. M. Krishnan, *IEEE Transactions on Medical Imaging*, 2015, **34**, 1077–1084.
154 S. Lou, J.-y. Ye, K.-q. Li and A. Wu, *Analyst*, 2012, **137**, 1174–1181.
155 R. M. Ferguson, A. P. Khandhar and K. M. Krishnan, *J. Appl. Phys.*, 2012, **111**, 07B318.
156 R. Hufschmid, H. Arami, R. M. Ferguson, M. Gonzales, E. Teeman, L. N. Brush, N. D. Browning and K. M. Krishnan, *Nanoscale*, 2015, **7**, 11142–11154.
157 Y. Geng, P. Dalhaimer, S. S. Cai, R. Tsai, M. Tewari, T. Minko and D. E. Discher, *Nat. Nanotechnol.*, 2007, **2**, 249–255.
158 Z. Liu, W. Cai, L. He, N. Nakayama, K. Chen, X. Sun, X. Chen and H. Dai, *Nat. Nanotechnol.*, 2006, **2**, 47–52.
159 Arnida, M. M. Janat-Amsbury, A. Ray, C. M. Peterson and H. Ghandehari, *Eur. J. Pharm. Biopharm.*, 2011, **77**, 417–423.
160 R. A. Petros and J. M. DeSimone, *Nat. Rev. Drug Discovery*, 2010, **9**, 615–627.
161 J. H. Park, G. von Maltzahn, L. L. Zhang, M. P. Schwartz, E. Ruoslahti, S. N. Bhatia and M. J. Sailor, *Adv. Mater.*, 2008, **20**, 1630–1635.
162 L. Zhan, G. Yanxia, Z. Xiaoyong, Q. Wei, F. Qiaohui, L. Yan, J. Zongxian, W. Jianjun, T. Yuqin, D. Xiaojiang and W. Wangsuo, *J. Nanopart. Res.*, 2010, **13**, 2939–2947.
163 S.-T. Yang, J. Luo, Q. Zhou and H. Wang, *Theranostics*, 2012, **2**, 271–282.
164 Y. Akiyama, T. Mori, Y. Katayama and T. Niidome, *Nanoscale Res. Lett.*, 2012, **7**, 565.
165 H. Wu, G. Liu, Y. Zhuang, D. Wu, H. Zhang, H. Yang, H. Hu and S. Yang, *Biomaterials*, 2011, **32**, 4867–4876.
166 F. Erogbogbo, K. T. Yong, R. Hu, W. C. Law, H. Ding, C. W. Chang, P. N. Prasad and M. T. Swihart, *ACS Nano*, 2010, **4**, 5131–5138.

167 M. P. Melancon, W. Lu, M. Zhong, M. Zhou, G. Liang, A. M. Elliott, J. D. Hazle, J. N. Myers, C. Li and R. J. Stafford, *Biomaterials*, 2011, **32**, 7600–7608.
168 H. Yang, Y. Zhuang, Y. Sun, A. Dai, X. Shi, D. Wu, F. Li, H. Hu and S. Yang, *Biomaterials*, 2011, **32**, 4584–4593.
169 J. Xie, F. Zhang, M. Aronova, L. Zhu, X. Lin, Q. Quan, G. Liu, G. Zhang, K.-Y. Choi, K. Kim, X. Sun, S. Lee, S. Sun, R. Leapman and X. Chen, *ACS Nano*, 2011, **5**, 3043–3051.
170 M. P. Melancon, A. Elliott, X. Ji, A. Shetty, Z. Yang, M. Tian, B. Taylor, R. J. Stafford and C. Li, *Invest. Radiol.*, 2011, **46**, 132–140.
171 T. Liu, S. X. Shi, C. Liang, S. D. Shen, L. Cheng, C. Wang, X. J. Song, S. Goel, T. E. Barnhart, W. B. Cai and Z. Liu, *ACS Nano*, 2015, **9**, 950–960.
172 X. X. He, F. Y. Liu, L. Liu, T. C. Duan, H. M. Zhang and Z. X. Wanq, *Mol. Pharmaceutics*, 2014, **11**, 738–745.
173 Y. Liu, T. C. Hughes, B. W. Muir, L. J. Waddington, T. R. Gengenbach, C. D. Easton, T. M. Hinton, B. A. Moffat, X. Hao and J. Qiu, *Biomaterials*, 2014, **35**, 378–386.
174 J. L. Campbell, J. Arora, S. F. Cowell, A. Garg, P. Eu, S. K. Bhargava and V. Bansal, *PLoS One*, 2011, **6**, e21857.
175 L. Lartigue, D. Alloyeau, J. Kolosnjaj-Tabi, Y. Javed, P. Guardia, A. Riedinger, C. Pechoux, T. Pellegrino, C. Wilhelm and F. Gazeaut, *ACS Nano*, 2013, **7**, 3939–3952.
176 G. Sinigaglia, M. Magro, G. Miotto, S. Cardillo, E. Agostinelli, R. Zboril, E. Bidollari and F. Vianello, *Int. J. Nanomed.*, 2012, **7**, 2249–2259.
177 R. Venerando, G. Miotto, M. Magro, M. Dallan, D. Baratella, E. Bonaiuto, R. Zboril and F. Vianello, *J. Phys. Chem. C*, 2013, **117**, 20320–20331.
178 M. Magro, R. Campos, D. Baratella, G. Lima, K. Hola, C. Divoky, R. Stollberger, O. Malina, C. Aparicio, G. Zoppellaro, R. Zboril and F. Vianello, *Chem. – Eur. J.*, 2014, **20**, 11913–11920.
179 J. Skopalik, K. Polakova, M. Havrdova, I. Justan, M. Magro, D. Milde, L. Knopfova, J. Smarda, H. Polakova, E. Gabrielova, F. Vianello, J. Michalek and R. Zboril, *Int. J. Nanomed.*, 2014, **9**, 5355–5372.
180 Q. Quan, J. Xie, H. Gao, M. Yang, F. Zhang, G. Liu, X. Lin, A. Wang, H. S. Eden, S. Lee, G. Zhang and X. Chen, *Mol. Pharmaceutics*, 2011, **8**, 1669–1676.
181 Q. Tong, H. Li, W. Li, H. Chen, X. Shu, X. Lu and G. Wang, *J. Nanosci. Nanotechnol.*, 2011, **11**, 3651–3658.
182 S. Garcia-Jimeno, E. Escribano, J. Queralt and J. Estelrich, *Int. J. Pharm.*, 2011, **405**, 181–187.
183 M. Gonzales, L. M. Mitsumori, J. V. Kushleika, M. E. Rosenfeld and K. M. Krishnan, *Contrast Media Mol. Imaging*, 2010, **5**, 286–293.
184 A. S. Karakoti, S. Das, S. Thevuthasan and S. Seal, *Angew. Chem., Int. Ed.*, 2011, 1980–1994.
185 T. Y. Liu, K. H. Liu, D. M. Liu, S. Y. Chen and I. W. Chen, *Adv. Funct. Mater.*, 2009, **19**, 616–623.
186 S. Purushotham, P. E. J. Chang, H. Rumpel, I. H. C. Kee, R. T. H. Ng, P. K. H. Chow, C. K. Tan and R. V. Ramanujan, *Nanotechnology*, 2009, **20**, 305101.
187 Y. X. Zhao, C. L. Wang, L. Wang, Q. Yang, W. Y. Tang, Z. N. She and Y. H. Deng, *Eur. J. Pharm. Biopharm.*, 2012, **81**, 506–513.
188 H. Xu, K. Q. Wang, Y. H. Deng and D. W. Chen, *Biomaterials*, 2010, **31**, 4757–4763.
189 T. Ishida and H. Kiwada, *Int. J. Pharm.*, 2008, **354**, 56–62.
190 T. Ishihara, M. Takeda, H. Sakamoto, A. Kimoto, C. Kobayashi, N. Takasaki, K. Yuki, K. I. Tanaka, M. Takenaga, R. Igarashi, T. Maeda, N. Yamakawa, Y. Okamoto, M. Otsuka, T. Ishida, H. Kiwada, Y. Mizushima and T. Mizushima, *Pharm. Res.*, 2009, **26**, 2270–2279.
191 E. Hara, A. Makino, K. Kurihara, F. Yamamoto, E. Ozeki and S. Kimura, *Int. Immunopharmacol.*, 2012, **14**, 261–266.
192 T. Suzuki, M. Ichihara, K. Hyodo, E. Yamamoto, T. Ishida, H. Kiwada, H. Ishihara and H. Kikuchi, *Int. J. Pharm.*, 2012, **436**, 636–643.
193 H. Wei, N. Insin, J. Lee, H.-S. Han, J. M. Cordero, W. Liu and M. G. Bawendi, *Nano Lett.*, 2012, **12**, 22–25.
194 A. J. Keefe and S. Jiang, *Nat. Chem.*, 2012, **4**, 59–63.
195 Y. Zhang, J.-Y. Liu, S. Ma, Y.-J. Zhang, X. Zhao, X.-D. Zhang and Z.-D. Zhang, *J. Mater. Sci.: Mater. Med.*, 2010, **21**, 1205–1210.
196 K. Knop, R. Hoogenboom, D. Fischer and U. S. Schubert, *Angew. Chem., Int. Ed.*, 2010, **49**, 6288–6308.
197 R. R. Arvizo, O. R. Miranda, D. F. Moyano, C. A. Walden, K. Giri, R. Bhattacharya, J. D. Robertson, V. M. Rotello, J. M. Reid and P. Mukherjee, *PLoS One*, 2011, **6**, e24374.
198 Q. Yang, S. W. Jones, C. L. Parker, W. C. Zamboni, J. E. Bear and S. K. Lai, *Mol. Pharmaceutics*, 2014, **11**, 1250–1258.
199 D. E. Owens and N. A. Peppas, *Int. J. Pharm.*, 2006, **307**, 93–102.
200 S. M. Moghimi and J. Szebeni, *Prog. Lipid Res.*, 2003, **42**, 463–478.
201 K. Ujiie, N. Kanayama, K. Asai, M. Kishimoto, Y. Ohara, Y. Akashi, K. Yamada, S. Hashimoto, T. Oda, N. Ohkohchi, H. Yanagihara, E. Kita, M. Yamaguchi, H. Fujii and Y. Nagasaki, *Colloids Surf., B*, 2011, **88**, 771–778.
202 C. Passirani and J.-P. Benoit, *Biomaterials for Delivery and Targeting of Proteins and Nucleic Acids*, CRC Press, Boca Raton, Florida, 2005.
203 W. D. Callister and D. G. Rethwisch, *Fundamentals of Materials Science and Engineering*, Wiley, Hoboken, New Jersy, 2011.
204 K. Kunal, C. G. Robertson, S. Pawlus, S. F. Hahn and A. P. Sokolov, *Macromolecules*, 2008, **41**, 7232–7238.
205 H. Chen, L. Wang, J. Yeh, X. Wu, Z. Cao, Y. A. Wang, M. Zhang, L. Yang and H. Mao, *Biomaterials*, 2010, **31**, 5397–5407.
206 P. P. Karmali, Y. Chao, J. H. Park, M. J. Sailor, E. Ruoslahti, S. C. Esener and D. Simberg, *Mol. Pharmaceutics*, 2012, **9**, 539–545.
207 M. F. Bellin, C. Roy, K. Kinkel, D. Thoumas, S. Zaim, D. Vanel, C. Tuchmann, F. Richard, D. Jacqmin, A. Delcourt, E. Challier, T. Lebret and P. Cluzel, *Radiology*, 1998, **207**, 799–808.
208 L. Josephson, C. H. Tung, A. Moore and R. Weissleder, *Bioconjugate Chem.*, 1999, **10**, 186–191.

209 M. Mahmoudi, S. Sheibani, A. S. Milani, F. Rezaee, M. Gauberti, R. Dinarvand and H. Vali, *Nanomedicine*, 2015, **10**, 215–226.
210 T. L. Doane, C. H. Chuang, R. J. Hill and C. Burda, *Acc. Chem. Res.*, 2012, **45**, 317–326.
211 J. C. Berg, *An Introduction to Interfaces and Colloids*, World Scientific Publishing Co., Singapore, 2010.
212 N. B. Shah, G. M. Vercellotti, J. G. White, A. Fegan, C. R. Wagner and J. C. Bischof, *Mol. Pharmaceutics*, 2012, **9**, 2146–2155.
213 C. Sun, J. S. H. Lee and M. Zhang, *Adv. Drug Delivery Rev.*, 2008, **60**, 1252.
214 L. Maurizi, A. L. Papa, L. Dumont, F. Bouyer, P. Walker, D. Vandroux and N. Millot, *J. Biomed. Nanotechnol.*, 2015, **11**, 126–136.
215 B. Chertok, A. E. David and V. C. Yang, *Biomaterials*, 2010, **31**, 6317–6324.
216 U. Sakulkhu, M. Mahmoudi, L. Maurizi, J. Salaklang and H. Hofmann, *Sci. Rep.*, 2014, **4**.
217 C. Schweiger, R. Hartmann, F. Zhang, W. J. Parak, T. H. Kissel and P. Rivera Gil, *J. Nanobiotechnol.*, 2012, **10**.
218 S. Metz, G. Bonaterra, M. Rudelius, M. Settles, E. J. Rummeny and H. E. Daldrup-Link, *Eur. Radiol.*, 2004, **14**, 1851–1858.
219 S. Nagayama, K. Ogawara, Y. Fukuoka, K. Higaki and T. Kimura, *Int. J. Pharm.*, 2007, **342**, 215–221.
220 P. Aggarwal, J. B. Hall, C. B. McLeland, M. A. Dobrovolskaia and S. E. McNeil, *Adv. Drug Delivery Rev.*, 2009, **61**, 428–437.
221 U. Sakulkhu, M. Mahmoudi, L. Maurizi, G. Coullerez, M. Hofmann-Amtenbrink, M. Vries, M. Motazacker, F. Rezaee and H. Hofmann, *Biomater. Sci.*, 2015, **3**, 265–278.
222 M. Mahmoudi and V. Serpooshan, *J. Phys. Chem. C*, 2011, **115**, 18275–18283.
223 M. Mahmoudi, I. Lynch, M. R. Ejtehadi, M. P. Monopoli, F. B. Bombelli and S. Laurent, *Chem. Rev.*, 2011, **111**, 5610–5637.
224 A. M. W. Reed and S. J. Metallo, *Langmuir*, 2010, **26**, 18945–18950.
225 P. P. Karmali and D. Simberg, *Expert Opin. Drug Delivery*, 2011, **8**, 343–357.
226 H. H. P. Yiu, *Nanomedicine*, 2011, **6**, 1429–1446.
227 I. T. Lucas, S. Durand-Vidal, E. Dubois, J. Chevalet and P. Turq, *J. Phys. Chem. C*, 2007, **111**, 18568–18576.
228 G. W. Simmons and B. C. Beard, *J. Phys. Chem.*, 1987, **91**, 1143–1148.
229 S. Wildermuth, B. Dubno, J. Romanowski, A. Borseth, A. Annweiler and J. F. Debatin, in *Sixth Annual Scientific Meeting of the International Society of Magnetic Resonance in Medicine (ISMRM)*, Sidney, 1998.
230 H. Jackson, O. Muhammad, H. Daneshvar, J. Nelms, A. Popescu, M. A. Vogelbaum, M. Bruchez and S. A. Toms, *J. Neuro-Oncol.*, 2008, **87**, 243.
231 V. Dousset, C. Gomez, K. G. Petry, C. Delalande and J.-M. Caille, *Magn. Reson. Mater. Phys., Biol. Med.*, 1999, **8**, 185–189.
232 M. M. Bailey and C. J. Berkland, *Med. Res. Rev.*, 2009, **29**, 196–212.
233 A. A. Faraj, A. P. Shaik and A. S. Shaik, *Nanotoxicology*, 2014, 1–10, Early Oline.
234 A. R. Martin, R. B. Thompson and W. H. Finlay, *J. Aerosol Med. Pulm. Drug Delivery*, 2008, **21**, 335–341.
235 A. Al Faraj, G. Lacroix, H. Alsaid, D. Elgrabi, V. Stupar, F. Robidel, S. Gaillard, E. Canet-Soulas and Y. Cremillieux, *Magn. Reson. Med.*, 2008, **59**, 1298–1303.
236 W. S. Cho, M. J. Cho, S. R. Kim, M. Choi, J. Y. Lee, B. S. Han, S. N. Park, M. K. Yu, S. Jon and J. Jeong, *Toxicol. Appl. Pharmacol.*, 2009, **239**, 106–115.
237 J. L. Turi, F. M. Yang, M. D. Garrick, C. A. Piantadosi and A. J. Ghio, *Free Radicals Biol. Med.*, 2004, **36**, 850–857.
238 E. A. Heilig, K. J. Thompson, R. M. Molina, A. R. Ivanov, J. D. Brain and M. Wessling-Resnick, *Am. J. Physiol.: Lung Cell. Mol. Physiol.*, 2006, **290**, L1247–L1259.
239 C. R. A. Valois, J. M. Braz, E. S. Nunes, M. A. R. Vinolo, E. C. D. Lima, R. Curi, W. M. Kuebler and R. B. Azevedo, *Biomaterials*, 2010, **31**, 366–374.
240 F. W. Merkus and M. P. v. d. Berg, *Drugs R&D*, 2007, **8**, 133–144.
241 B. Wang, W. Y. Feng, M. Wang, J. W. Shi, F. Zhang, H. Ouyang, Y. L. Zhao, Z. F. Chai, Y. Y. Huang, Y. N. Xie, H. F. Wang and J. Wang, *Biol. Trace Elem. Res.*, 2007, **118**, 233–243.
242 D. B. Rao, B. A. Wong, B. E. McManus, A. M. McElveen, A. R. James and D. C. Dorman, *Toxicol. Appl. Pharmacol.*, 2003, **193**, 116–126.
243 J. T. Kwon, S. K. Hwang, H. Jin, D. S. Kim, A. Mina-Tehrani, H. J. Yoon, M. Chop, T. J. Yoon, D. Y. Han, Y. W. Kang, B. I. Yoon, J. K. Lee and M. H. Cho, *J. Occup. Health*, 2008, **50**, 1–6.
244 J. T. Kwon, D. S. Kim, A. Minai-Tehrani, S. K. Hwang, S. H. Chang, E. S. Lee, C. X. Xu, H. T. Lim, J. E. Kim, B. I. Yoon, G. H. An, K. H. Lee, J. K. Lee and M. H. Cho, *J. Occup. Health*, 2009, **51**, 423–431.
245 C. Geraldes and S. Laurent, *Contrast Media Mol. Imaging*, 2009, **4**, 1–23.
246 P. F. Hahn, D. D. Stark, J. M. Lewis, S. Saini, G. Elizondo, R. Weissleder, C. J. Fretz and J. T. Ferrucci, *Radiology*, 1990, **175**, 695–700.
247 R. C. H. Heusler, E. Wight and B. Marincek, *J. Magn. Reson. Imaging*, 1995, **5**, 385–391.
248 J. J. Cheng, B. A. Teply, S. Y. Jeong, C. H. Yim, D. Ho, I. Sherifi, S. Jon, O. C. Farokhzad, A. Khademhosseini and R. S. Langer, *Pharm. Res.*, 2006, **23**, 557–564.
249 M. Goldberg and I. Gomez-Orellana, *Nat. Rev. Drug Discovery*, 2003, **2**, 289–295.
250 H. D. Singh, S. Roychowdhury, P. Verma and V. Bhandari, *IOSR J. Pharm.*, 2012, **2**, 5–11.
251 J. Huang, Q. Shu, L. Y. Wang, H. Wu, A. Y. Wang and H. Mao, *Biomaterials*, 2015, **39**, 105–113.
252 J. T. Sockolosky, M. R. Tiffany and F. C. Szoka, *Proc. Natl. Acad. Sci. U. S. A.*, 2012, **109**, 16095–16100.
253 C. A. Smith, C. A. Simpson, G. Kim, C. J. Carter and D. L. Feldheim, *ACS Nano*, 2013, **7**, 3991–3996.
254 J. R. Kanwar, K. Roy and R. K. Kanwar, *Crit. Rev. Biochem. Mol. Biol.*, 2011, **46**, 459–477.

255 K. Tsuchiya, N. Nitta, A. Sonoda, A. Nitta-Seko, S. Ohta, H. Otani, M. Takahashi, K. Murata, K. Murase, S. Nohara and K. Mukaisho, *Int. J. Nanomed.*, 2011, **6**, 1–8.
256 J. S. Kim, T. J. Yoon, B. G. Kim, S. J. Park, H. W. Kim, K. H. Lee, S. B. Park, J. K. Lee and M. H. Cho, *Toxicol. Sci.*, 2006, **89**, 338–347.
257 W. W. Wu, B. A. Chen, J. A. Cheng, J. Wang, W. L. Xu, L. J. Liu, G. H. Xia, H. L. Wei, X. M. Wang, M. M. Yang, L. Y. Yang, Y. Zhang, C. L. Xu and J. Y. Li, *Int. J. Nanomed.*, 2010, **5**, 1079–1084.
258 H. B. Raju, Y. Hu, K. R. Padgett, J. E. Rodriguez and J. L. Goldberg, *Clin. Exp. Ophthalmol.*, 2012, **40**, 100–107.
259 J. Harrison, C. A. Bartlett, G. Cowin, P. K. Nicholls, C. W. Evans, T. D. Clemons, B. Zdyrko, I. A. Luzinov, A. R. Harvey, K. S. Iyer, S. A. Dunlop and M. Fitzgerald, *Small*, 2012, **8**, 1579–1589.
260 F. Gardikiotis, C. Peptu, M. Popa and D. Costin, *Oftalmologia*, 2011, **55**, 92–96.
261 K. Pusic, Z. Aguilar, J. McLoughlin, S. Kobuch, H. Xu, M. Tsang, A. Wang and G. Hui, *FASEB J.*, 2013, **27**, 1153–1166.
262 L. Johnson, S. E. Pinder and M. Douek, *Histopathology*, 2013, **62**, 481–486.
263 D. J. Grootendorst, J. Jose, R. M. Fratila, M. Visscher, A. H. Velders, B. Ten Haken, T. G. Van Leeuwen, W. Steenbergen, S. Manohar and T. J. M. Ruers, *Contrast Media Mol. Imaging*, 2013, **8**, 83–91.
264 Z. R. Stephen, F. M. Kievit, O. Veiseh, P. A. Chiarelli, C. Fang, K. Wang, S. J. Hatzinger, R. G. Ellenbogen, J. R. Silber and M. Q. Zhang, *ACS Nano*, 2014, **8**, 10383–10395.
265 E. Corem-Salkmon, Z. Ram, D. Daniels, B. Perlstein, D. Last, S. Salomon, G. Tamar, R. Shneor, D. Guez, S. Margel and Y. Mardor, *Int. J. Nanomed.*, 2011, **6**, 1595–1602.
266 G. De Rosa, G. Salzano, M. Caraglia and A. Abbruzzese, *Curr. Drug Metab.*, 2012, **13**, 61–69.
267 S. L. Raut, B. Kirthivasan, M. M. Bommana, E. Squillante and M. Sadoqi, *Nanotechnology*, 2010, **21**, 395102.
268 E. A. Rozhkova, *Adv. Mater.*, 2011, **23**, H136–H150.
269 R. Chen, G. Romero, M. G. Christiansen, A. Mohr and P. Anikeeva, *Science*, 2015, **347**, 1477–1480.
270 R. D. O. Engberink, E. L. A. Blezer, C. D. Dijkstra, S. M. A. van der Pol, A. van der Toorn and H. E. de Vries, *NMR Biomed.*, 2010, **23**, 1087–1096.
271 C. Petters, E. Irrsack, M. Koch and R. Dringen, *Neurochem. Res.*, 2014, **39**, 1648–1660.
272 C. L. Stanfield and W. J. Germann, *Principles of Human Physiology*, Pearson Education Inc., San Francisco, 3rd edn, 2008.
273 K. Cho, X. Wang, S. Nie, Z. Chen and D. M. Shin, *Clin. Cancer Res.*, 2008, **14**, 1310.
274 H. Sarin, A. S. Kanevsky, H. T. Wu, A. A. Sousa, C. M. Wilson, M. A. Aronova, G. L. Griffiths, R. D. Leapman and H. Q. Vo, *J. Transl. Med.*, 2009, **7**.
275 Z. Poon, J. B. Lee, S. W. Morton and P. T. Hammond, *Nano Lett.*, 2011, **11**, 2096–2103.
276 R. K. Jain and T. Stylianopoulos, *Nat. Rev. Clin. Oncol.*, 2010, **7**, 653–664.
277 R. Ranganathan, S. Madanmohan, A. Kesavan, G. Baskar, Y. R. Krishnamoorthy, R. Santosham, D. Ponraju, S. K. Rayala and G. Venkatraman, *Int. J. Nanomed.*, 2012, **7**, 1043–1060.
278 E. Gultepe, F. J. Reynoso, A. Jhaveri, P. Kulkarni, D. Nagesha, C. Ferris, M. Harisinghani, R. B. Campbell and S. Sridhar, *Nanomedicine*, 2010, **5**, 1173–1182.
279 S. D. Perrault, C. Walkey, T. Jennings, H. C. Fischer and W. C. W. Chan, *Nano Lett.*, 2009, **9**, 1909–1915.
280 M. Yu and J. Zheng, *ACS Nano*, 2015, **9**, 6655–6674.
281 L. Agemy, K. N. Sugahara, V. R. Kotamraju, K. Gujraty, O. M. Girard, Y. Kono, R. F. Mattrey, J.-H. Park, M. J. Sailor, A. I. Jimenez, C. Cativiela, D. Zanuy, F. J. Sayago, C. Aleman, R. Nussinov and E. Ruoslahti, *Blood*, 2010, **116**, 2847–2856.
282 F. Yamashita and M. Hashida, *Adv. Drug Delivery Rev.*, 2013, **65**, 139–147.
283 C. Plank, *Nat. Nanotechnol.*, 2009, **4**, 544–545.
284 M. L. M. Pisciotti, E. Lima, M. V. Mansilla, V. E. Tognoli, H. E. Troiani, A. A. Pasa, T. B. Creczynski-Pasa, A. H. Silva, P. Gurman, L. Colombo, G. F. Goya, A. Lamagna and R. D. Zysler, *J. Biomed. Mater. Res., Part B*, 2014, **102**, 860–868.
285 N. Schleich, C. Po, D. Jacobs, B. Ucakar, B. Gallez, F. Danhier and V. Preat, *J. Controlled Release*, 2014, **194**, 82–91.
286 M. G. Krukemeyer, V. Krenn, M. Jakobs and W. Wagner, *J. Surg. Res.*, 2012, **175**, 35–43.
287 H.-C. Huang, S. Barua, G. Sharma, S. K. Dey and K. Rege, *J. Controlled Release*, 2011, **155**, 344–357.
288 W. C. Zamboni, V. Torchilin, A. K. Patri, J. Hrkach, S. Stern, R. Lee, A. Nel, N. J. Panaro and P. Grodzinski, *Clin. Cancer Res.*, 2012, **18**, 3229–3241.
289 S. E. Lee, K. J. Choi, G. K. Menon, H. J. Kim, E. H. Choi, S. K. Ahn and S. H. Lee, *J. Invest. Dermatol.*, 2010, **130**, 1063–1072.
290 B. Baroli, M. G. Ennas, F. Loffredo, M. Isola, R. Pinna and M. A. Lopez-Quintela, *J. Invest. Dermatol.*, 2007, **127**, 1701–1712.
291 O. Ziv-Polat, M. Topaz, T. Brosh and S. Margel, *Biomaterials*, 2010, **31**, 741–747.
292 E. Alphandery, S. Faure, O. Seksek, F. Guyot and I. Chebbi, *ACS Nano*, 2011, **5**, 6279–6296.
293 J. Nissim, *Intravenous iron*, MD thesis, University of London, London, 1949.
294 G. W. Richter, *J. Exp. Med.*, 1959, **109**, 197–216.
295 A. S. Arbab, L. B. Wilson, P. Ashari, E. K. Jordan, B. K. Lewis and J. A. Frank, *NMR Biomed.*, 2005, **18**, 383–389.
296 Wahajuddin and S. Arora, *Int. J. Nanomed.*, 2012, **7**, 3445–3471.
297 O. Lunov, T. Syrovets, C. Roecker, K. Tron, G. U. Nienhaus, V. Rasche, V. Mailaender, K. Landfester and T. Simmet, *Biomaterials*, 2010, **31**, 9015–9022.
298 K. C. Briley-Saebo, L. O. Johansson, S. O. Hustvedt, A. G. Haldorsen, A. Bjornerud, Z. A. Fayad and H. K. Ahlstrom, *Invest. Radiol.*, 2006, **41**, 560–571.

299 M.-Y. Hua, H.-L. Liu, H.-W. Yang, P.-Y. Chen, R.-Y. Tsai, C.-Y. Huang, I. C. Tseng, L.-A. Lyu, C.-C. Ma, H.-J. Tang, T.-C. Yen and K.-C. Wei, *Biomaterials*, 2011, **32**, 516–527.
300 H. Arami and K. M. Krishnan, *J. Appl. Phys.*, 2014, **115**, 17B306.
301 E. Okon, D. Pouliquen, P. Okon, Z. V. Kovaleva, T. P. Stepanova, S. G. Lavit, B. N. Kudryavtsev and P. Jallet, *Lab. Invest.*, 1994, **71**, 895–903.
302 K. Briley-Saebo, A. Bjornerud, D. Grant, H. Ahlstrom, T. Berg and G. M. Kindberg, *Cell and Tissue Research*, 2004, **316**, 315–323.
303 K. Briley-Saebo, S. A. Hustvedt, A. Haldorsen and A. Bjornerud, *J. Magn. Reson. Imaging*, 2004, **20**, 622–631.
304 J. H. Jensen, H. Y. Tang, C. L. Tosti, S. V. Swaminathan, A. Nunez, K. Hultman, K. U. Szulc, E. X. Wu, D. Kim, S. Sheth, T. R. Brown and G. M. Brittenham, *Magn. Reson. Med.*, 2010, **63**, 1201–1209.
305 A. Singh, T. Patel, J. Hertel, M. Bernardo, A. Kausz and L. Brenner, *Am. J. Kidney Dis.*, 2008, **52**, 907–915.
306 E. Sarac, N. Haroon, J. John and D. Gemmel, *Am. J. Kidney Dis.*, 2012, **59**, A74.
307 S. Shanehsazzadeh, M. A. Oghabian, F. J. Daha, M. Amanlou and B. J. Allen, *J. Radioanal. Nucl. Chem.*, 2013, **295**, 1517–1523.
308 M. Ahmd, K. Rashid, M. Nadeem, K. Masood, S. Ali, M. Nafees, N. Gull, Mumtaz-ul-Haq, N. Ibrahim, A. Saeed, A. Qureshy, F. Aleem, H. Naseer, S. Mehmood and S. W. Hyder, *J. Colloid Sci. Biotechnol.*, 2012, **1**, 201–209.
309 R. Chakravarty, H. F. Valdovinos, F. Chen, C. M. Lewis, P. A. Ellison, H. Luo, M. E. Meyerand, R. J. Nickles and W. Cai, *Adv. Mater.*, 2014, **26**, 5119–5123.
310 B. Freund, U. I. Tromsdorf, O. T. Bruns, M. Heine, A. Giemsa, A. Bartelt, S. C. Salmen, N. Raabe, J. Heeren, H. Ittrich, R. Reimer, H. Hohenberg, U. Schumacher, H. Weller and P. Nielsen, *ACS Nano*, 2012, **6**, 7318–7325.
311 H. T. Wang, R. Kumar, D. Nagesha, R. I. Duclos, S. Sridhar and S. J. Gatley, *Nucl. Med. Biol.*, 2015, **42**, 65–70.
312 P. Bourrinet, H. H. Bengele, B. Bonnemain, A. Dencausse, J. M. Idee, P. M. Jacobs and J. M. Lewis, *Invest. Radiol.*, 2006, **41**, 313–324.
313 J. A. Tate, A. A. Petryk, A. J. Giustini and P. J. Hoopes, *Proc. SPIE*, 2011, **7901**, 1–9.
314 J. M. Berg, J. L. Tymoczko and L. Stryer, *Biochemistry*, W H Freeman, New York, 5th edn, 2002.
315 X. L. Zhang, C. S. Liu, Y. Yuan, X. Q. Shan, Y. Sheng and F. Xu, *J. Biomed. Mater. Res., Part B*, 2008, **87B**, 354–363.
316 A. Hanini, A. Schmitt, K. Kacem, F. Chau, S. Ammar and J. Gavard, *Int. J. Nanomed.*, 2011, **6**, 787–794.
317 C. Geers and G. Gros, *Physiol. Rev.*, 2000, **80**, 681–715.
318 X. Q. Yang, H. Hong, J. J. Grailer, I. J. Rowland, A. Javadi, S. A. Hurley, Y. L. Xiao, Y. A. Yang, Y. Zhang, R. Nickles, W. B. Cai, D. A. Steeber and S. Q. Gong, *Biomaterials*, 2011, **32**, 4151–4160.
319 L. L. C. Estevanato, L. M. Lacava, L. C. F. Carvalho, R. B. Azevedo, O. Silva, F. Pelegrini, S. N. Bao, P. C. Morais and Z. G. M. Lacava, *J. Biomed. Nanotechnol.*, 2012, **8**, 301–308.
320 B. Chertok, A. J. Cole, A. E. David and V. C. Yang, *Mol. Pharmaceutics*, 2010, **7**, 375–385.
321 A. J. Giustini, R. Ivkov and P. J. Hoopes, *Nanotechnology*, 2011, **22**, 345101.
322 M. Thaler, S. Roy, A. Fornara, M. Bitsche, J. Qin, M. Muhammed, W. Salvenmoser, G. Rieger, A. S. Fischer and R. Glueckert, *Nanomedicine-Nanotechnology Biology and Medicine*, 2011, **7**, 360–369.
323 R. T. M. de Rosales, R. Tavare, A. Glaria, G. Varma, A. Protti and P. J. Blower, *Bioconjugate Chem.*, 2011, **22**, 455–465.
324 L. Maurizi, U. Sakulkhu, A. Gramoun, J. P. Vallee and H. Hofmann, *Analyst*, 2014, **139**, 1184–1191.
325 J. Zhuang, K. L. Fan, L. Z. Gao, D. Lu, J. Feng, D. L. Yang, N. Gu, Y. Zhang, M. M. Liang and X. Y. Yan, *Mol. Pharmaceutics*, 2012, **9**, 1983–1989.
326 H. Ding and F. Wu, *Theranostics*, 2012, **2**, 1040–1053.
327 P. J. Hoopes, A. A. Petryka, B. Gimib, A. J. Giustini, J. B. Weaver, J. Bischof, R. Chamberlaine and M. Garwoode, *Proc. SPIE*, 2012, **8317**, 83170R83171.
328 P. W. Goodwill, E. U. Saritas, L. R. Croft, T. N. Kim, K. M. Krishnan, D. V. Schaffer and S. M. Conolly, *Adv. Mater.*, 2012, **24**, 3870–3877.
329 B. Gleich and J. Weizenecker, *Nature*, 2005, **435**, 1214–1217.
330 R. M. Ferguson, A. P. Khandhar, H. Arami, L. Hua, O. Hovorka and K. M. Krishnan, *Biomed. Eng.*, 2013, **58**, 493–507.
331 L. M. Bauer, S. F. Situ, M. A. Griswold and A. C. S. Samia, *J. Phys. Chem. Lett.*, 2015, **6**, 2509–2517.
332 H. Mok, O. Veiseh, C. Fang, F. M. Kievit, F. Y. Wang, J. O. Park and M. Q. Zhang, *Mol. Pharmaceutics*, 2010, **7**, 1930–1939.
333 M. Bellusci, A. La Barbera, F. Padella, M. Mancuso, A. Pasquo, M. G. Grollino, G. Leter, E. Nardi, C. Cremisini, P. Giardullo and F. Pacchierotti, *Int. J. Nanomed.*, 2014, **9**, 1919–1929.
334 L. F. Gamarra, A. J. daCosta-Filho, J. B. Mamani, R. d. C. Ruiz, L. F. Pavon, T. T. Sibov, E. D. Vieira, A. C. Silva, W. M. Pontuschka and E. Amaro Jr, *Int. J. Nanomed.*, 2010, **5**, 203–211.
335 N. Raabe, E. Forberich, B. Freund, O. T. Bruns, M. Heine, M. G. Kaul, U. Tromsdorf, L. Herich, P. Nielsen, R. Reimer, H. Hohenberg, H. Weller, U. Schumacher, G. Adam and H. Ittrich, *Contrast Media Mol. Imaging*, 2015, **10**, 153–162.
336 J. F. Zeng, B. Jia, R. R. Qiao, C. Wang, L. H. Jing, F. Wang and M. Y. Gao, *Chem. Commun.*, 2014, **50**, 2170–2172.
337 D. Bargheer, A. Giemsa, B. Freund, M. Heine, C. Waurisch, G. M. Stachowski, S. G. Hickey, A. Eychmueller, J. Heeren and P. Nielsen, *Beilstein J. Nanotechnol.*, 2015, **6**, 111–123.
338 E.-J. Cha, E. S. Jang, I.-C. Sun, I. J. Lee, J. H. Ko, Y. I. Kim, I. C. Kwon, K. Kim and C.-H. Ahn, *J. Controlled Release*, 2011, **155**, 152–158.
339 S. P. Foy, R. L. Manthe, S. T. Foy, S. Dimitrijevic, N. Krishnamurthy and V. Labhasetwar, *ACS Nano*, 2010, **4**, 5217–5224.
340 S. H. Crayton, D. R. Elias, A. Al Zaki, Z. Cheng and A. Tsourkas, *Biomaterials*, 2012, **33**, 1509–1519.
341 P. C. Naha, A. Al Zaki, E. Hecht, M. Chorny, P. Chhour, E. Blankemeyer, D. M. Yates, W. R. T. Witschey, H. I. Litt,

A. Tsourkas and D. P. Cormode, *J. Mater. Chem. B*, 2014, **2**, 8239–8248.
342 M. Li and J. Reineke, *Nanotoxicity: Methods and Protocols, Methods in Molecular Biology*, 2012, **926**, 369–382.
343 S. Wada, L. Yue, K. Tazawa, I. Furuta, H. Nagae, S. Takemori and T. Minamimura, *Oral Diseases*, 2001, **7**, 192–195.
344 S. Puntarulo, *Mol. Aspects Med.*, 2005, **26**, 299–312.
345 S. J. H. Soenen and M. De Cuyper, *Nanomedicine*, 2010, **5**, 1261–1275.
346 V. Monge-Fuentes, M. P. Garcia, M. C. H. Tavares, C. R. A. Valois, E. C. D. Lima, D. S. Teixeira, P. C. Morais, C. Tomaz and R. B. Azevedo, *Nanomedicine*, 2011, **6**, 1529–1544.
347 T. K. Jain, M. K. Reddy, M. A. Morales, D. L. Leslie-Pelecky and V. Labhasetwar, *Mol. Pharmaceutics*, 2008, **5**, 316–327.
348 R. Mejias, S. Perez-Yaguee, L. Gutierrez, L. I. Cabrera, R. Spada, P. Acedo, C. J. Serna, F. J. Lazaro, A. Villanueva, M. del Puerto Morales and D. F. Barber, *Biomaterials*, 2011, **32**, 2938–2952.
349 S. B. Chaves, L. M. Lacava, Z. G. M. Lacava, O. Silva, F. Pelegrini, N. Buske, C. Gansau, P. C. Morais and R. B. Azevedo, *IEEE Trans. Magn.*, 2002, **38**, 3231–3233.
350 R. Mejias, S. Perez-Yaguee, A. G. Roca, N. Perez, A. Villanueva, M. Canete, S. Manes, J. Ruiz-Cabello, M. Benito, A. Labarta, X. Batlle, S. Veintemillas-Verdaguer, M. Puerto Morales, D. F. Barber and C. J. Serna, *Nanomedicine*, 2010, **5**, 397–408.
351 J. H. Feng, H. L. Liu, L. M. Zhang, K. Bhakoo and L. H. Lu, *Nanotechnology*, 2010, **21**, 395101.
352 J. H. Feng, H. L. Liu, K. K. Bhakoo, L. H. Lu and Z. Chen, *Biomaterials*, 2011, **32**, 6558–6569.
353 E. J. Park, H. Kim, Y. Kim, J. Yi, K. Choi and K. Park, *Toxicology*, 2010, **275**, 65–71.
354 G. Masselli and G. Gualdi, *Radiology*, 2012, **264**, 333–348.
355 J. Wang, B. Chen, N. Jin, G. Xia, Y. Chen, Y. Zhou, X. Cai, J. Ding, X. Li and X. Wang, *Int. J. Nanomed.*, 2011, **6**, 605–610.
356 M. Kumari, S. Rajak, S. P. Singh, S. I. Kumari, P. U. Kumar, U. S. N. Murty, M. Mahboob, P. Grover and M. F. Rahman, *J. Nanosci. Nanotechnol.*, 2012, **12**, 2149–2159.
357 K. R. Di Bona, Y. Xu, P. A. Ramirez, J. DeLaine, C. Parker, Y. Bao and J. F. Rasco, *Reprod. Toxicol.*, 2014, **50**, 36–42.
358 P. L. McCormack, *Drugs*, 2012, **72**, 2013–2022.
359 S. Motoyama, K. Ishiyama, K. Maruyama, K. Narita, Y. Minamiya and J.-i. Ogawa, *World J. Surg.*, 2012, **36**, 83–89.
360 S. P. S. Howarth, T. Y. Tang, R. Trivedi, R. Weerakkody, J. U-King-Im, M. E. Gaunt, J. R. Boyle, Z. Y. Li, S. R. Miller, M. J. Graves and J. H. Gillard, *Eur. J. Radiol.*, 2009, **70**, 555–560.
361 H. Bernd, E. De Kerviler, S. Gaillard and B. Bonnemain, *Invest. Radiol.*, 2009, **44**, 336–342.
362 *Rienso (ferumoxytol): summary of product characteristics*, Takeda Global Research and Development Centre (Europe) Ltd, London, 2012.
363 S. Fishbane, W. K. Bolton, W. C. Winkelmayer, W. Strauss, Z. Li and B. J. G. Pereira, *Clin. Nephrol.*, 2012, **78**, 181–188.
364 D. Hasan, N. Chalouhi, P. Jabbour, A. S. Dumont, D. K. Kung, V. A. Magnotta, W. L. Young, T. Hashimoto, H. R. Winn and D. Heistad, *Stroke*, 2012, **43**, 3258–3265.
365 B. Schiller, P. Bhat and A. Sharma, *et al.*, American Society of Nephrology Kidney, Philadelphia (PA), 2011.
366 A. Barton Pai and A. O. Garba, *J. Blood Med.*, 2012, **3**, 77–85.
367 J. Nissim, *Guy's Hosp. Rep.*, 1953, **102**, 164–179.